

Diffuse atomic reflection at a rough mirror

Carsten Henkel,¹ Klaus Mølmer,² Robin Kaiser,¹ Nathalie Vansteenkiste,¹ Christoph I. Westbrook,¹ and Alain Aspect¹

¹*Institut d'Optique, Unité de Recherche No. 14 associée au CNRS, Boîte Postale 147, 91403 Orsay CEDEX, France*

²*Institute of Physics and Astronomy, University of Aarhus, 8000 Århus C, Denmark*

(Received 18 September 1996)

We present a theoretical analysis of the influence of surface roughness on the atomic reflection from an evanescent wave mirror. In our calculations we assume that light scattered at the rough dielectric surface interferes with the evanescent wave, creating a rough potential that scatters the atoms. We calculate the probability of diffuse reflection and the momentum distribution of the scattered atoms with a statistical model for the rough surface. The atomic reflection is diffuse rather than specular if the surface roughness is comparable to the wavelength of the incident atoms. We discuss the spatial coherence of the reflected matter waves. We indicate how to generalize our treatment to the case of multilevel atoms. [S1050-2947(97)04002-X]

PACS number(s): 03.75.Be, 34.50.-s, 39.20.+q, 68.35.Ct

I. INTRODUCTION

Mirrors are key components of optical devices for both electromagnetic and matter waves. In particular for interferometric applications, it is important to ensure that the reflection at the mirror is specular, since diffuse scattering is equivalent to a loss of spatial coherence of the reflected wave. This means that the roughness of the mirror surface must be kept below the wavelength of the incident wave. The constraints on surface quality required for matter wave mirrors are therefore more stringent than for optical mirrors if the de Broglie wavelength is smaller than the optical wavelength. This situation is frequently encountered in atom optics.

We discuss in this paper the diffuse reflection of atoms at an evanescent wave mirror. This device has been used in several atom optics experiments [1–7], including multiple reflection [8], diffraction [9–11], and interferometry [12]. The atoms are reflected by the repulsive optical potential of a blue detuned, evanescent light field above the surface of a dielectric prism. At a sufficiently large detuning, the excited-state population is small and hence the probability of spontaneous emission is negligible. Recently, however, we have obtained experimental evidence for a nonspecular reflection, depending on the quality of the prism surface [13]. In this experiment, a surface roughness on the angstrom scale was sufficient to cause a diffuse rather than specular reflection.

Although the optical potential of the evanescent wave prevents the atoms from interacting directly with the surface, several mechanisms are responsible for an indirect interaction. These include the interaction with stray light that is scattered from the prism, as well as the modification of the van der Waals–London–Casimir interaction due to the surface roughness. In this paper, we focus on one particular effect due to the light scattered at the prism surface: when this light interferes with the unscattered evanescent wave, it creates random spatial variations of the optical near-field intensity above the surface. The repulsive optical potential of the atomic mirror hence acquires some roughness, leading to a diffuse rather than specular reflection of the atoms.

In order to characterize the scattering of the atoms at the rough optical potential, we calculate the probability of dif-

fuse reflection and the atomic momentum distribution after reflection. Two different approaches are presented. First, we treat the scattering of the atomic wave by the rough part of the optical potential in first-order perturbation theory, using the Born approximation, i.e., assuming that a small fraction of the incident atoms is scattered. The atomic momentum distribution then contains a diffuse background that corresponds to the scattered atoms, in addition to a specularly reflected peak. We find that the probability of diffuse reflection is equal to the square of the ratio between an effective mirror roughness and the incident atomic wavelength. The effective roughness is interpreted as the roughness of the atomic “turning point surface,” i.e., the isopotential surface where the optical potential of the rough evanescent wave equals the incident kinetic energy. We find that the diffuse reflection of the atoms is similar to the scattering from an infinite potential barrier located at the rough turning point surface. This type of potential is known as the “corrugated hard wall” potential in the scattering of atoms from crystal-line surfaces [14–16]. We point out that the effective mirror roughness is comparable to the surface roughness of the dielectric prism. This implies that the prism surface must be smooth at the scale of the atomic wavelength for the reflection of the atoms at the evanescent wave mirror to be specular.

In a second approach, we use a thin phase grating approximation to take into account the rough optical potential. This approach is based on a semiclassical perturbation method [17] and has been developed for atomic diffraction by a standing evanescent wave [18,19]. It is equivalent to the Raman-Nath approximation [20,21] for a transmission grating. The thin phase grating approximation allows us to go beyond the Born approximation and to cover the diffuse reflection regime where the surface roughness is larger than the incident atomic wavelength. In this regime, the momentum distribution of the reflected atoms contains no specular peak and is broader than in the quasispecular regime. It is interpreted as an average diffraction pattern for an incoherent ensemble of phase gratings with a large phase modulation.

In both the Born and the thin phase grating approximations, we apply a statistical description for the rough surface in order to compute the atomic scattering. We model the

surface profile by a random variable whose statistical averages are characterized by a correlation function. This statistical framework allows us to introduce in a natural manner the spatial coherence function of the reflected atoms. The coherence function characterizes the quality of the reflection when the evanescent wave mirror is used in an atom interferometer. It also allows to calculate the average momentum distribution of the reflected atoms by means of a Fourier transformation.

The outline of the paper is as follows. We first recall some results for the atomic reflection at a perfectly flat evanescent wave mirror in the small-saturation and large-detuning limit (Sec. II). We restrict ourselves in the beginning to a two-level atom and ignore the polarization of the light. The scattered light field above the rough surface is given in Sec. III, where we recall the results of a perturbative calculation to first order in the surface roughness [22–27]. In this section we also introduce the statistical model for the rough surface and discuss the validity conditions for the light field calculation.

The rough optical potential created by the interference of the scattered light with the evanescent wave is introduced and discussed in Sec. IV. In Sec. V we study the diffuse reflection of atoms at the rough potential by means of the first Born approximation. Section VI is devoted to the calculation of the atomic scattering in the thin phase grating approach. We show that this approximation recovers the results of the Born approximation in the quasispecular limit.

We finally outline in Sec. VII the generalization of the present approach when the light polarization and the atomic Zeeman sublevel structure are taken into account. This provides the atom optics analog of polarization-resolved light scattering at rough surfaces. The Appendixes give some results for the atomic motion in the flat evanescent wave mirror (Appendix A) and the scattering of vector electromagnetic waves at a rough dielectric surface (Appendix B) that are used in the text.

II. MODEL POTENTIAL FOR THE EVANESCENT WAVE MIRROR

A. Optical potential

In the limit of large detuning compared to the natural linewidth of the excited state and low saturation of the atomic transition, the reactive part of the atom-light interaction dominates over the dissipative part. We may then assume that the atom remains in its ground state, neglect spontaneous emission, and describe the atomic motion by the optical or dipole potential, i.e., the position-dependent light shift of the atomic ground state. To begin with, we consider a two-level atom and defer the discussion of polarization to Sec. VII. The optical potential then takes the form

$$V(\mathbf{r}) = \frac{d^2}{\hbar\Delta} E^*(\mathbf{r})E(\mathbf{r}), \quad (2.1)$$

where the detuning Δ is the difference between the light frequency ω_L and the atomic transition frequency, d is the atomic dipole moment, and $E(\mathbf{r})$ and $E^*(\mathbf{r})$ are the positive and negative frequency components of the electric field

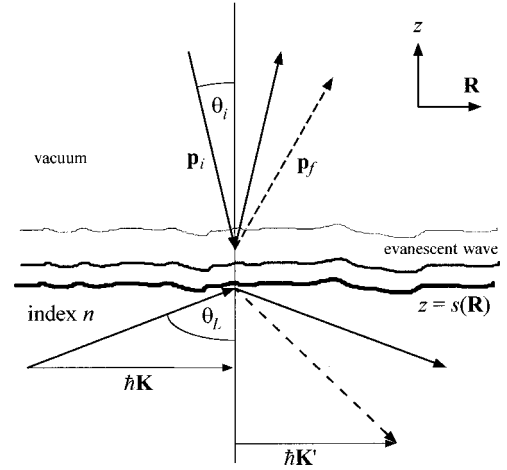


FIG. 1. Geometry of the problem. The totally internally reflected light beam is scattered by the rough surface. The scattered beam interferes with the evanescent wave, creating a rough evanescent wave. The roughness of the evanescent wave mirror renders the atomic reflection nonspecular.

$$E(\mathbf{r}, t) = E(\mathbf{r})e^{-i\omega_L t} + E^*(\mathbf{r})e^{i\omega_L t}. \quad (2.2)$$

We shall further suppose that the atom is moving sufficiently slowly so that the Doppler shift is negligible compared to the detuning. The optical potential (2.1) is then independent of the atomic velocity. Note that this approximation has to be reviewed for atoms that are reflected at grazing incidence [1,3–5].

B. Flat mirror

The evanescent wave is created by the total internal reflection of a plane light wave with an angle of incidence θ_L at the surface of a dielectric with refractive index n , as shown in Fig. 1. In the absence of surface roughness, the electric field in the vacuum above the surface $z=0$ is an evanescent wave

$$E^{(0)}(\mathbf{r}) = E_0 \exp(i\mathbf{K} \cdot \mathbf{R} - \kappa z), \quad \mathbf{r} = (\mathbf{R}, z), \quad (2.3)$$

where κ is given in terms of \mathbf{K} by

$$\kappa = \sqrt{|\mathbf{K}|^2 - k_L^2}. \quad (2.4)$$

We use bold capital letters \mathbf{K}, \mathbf{R} for vector components parallel to the surface. The electric-field amplitude E_0 at the surface is related to the incident field by a Fresnel transmission coefficient. The magnitude of the in-plane wave vector \mathbf{K} of the evanescent wave is $nk_L \sin \theta_L$, where $k_L = \omega_L/c$ is the magnitude of the optical wave vector in vacuum. The decay length $1/\kappa$ of the evanescent wave is of the order of the reduced optical wavelength $\lambda_L/2\pi$, unless the light wave inside the dielectric is close to the critical angle.

For a positive detuning Δ , the optical potential of the flat evanescent wave (2.3) is a repulsive barrier that varies exponentially as a function of the distance from the surface

$$V^{(0)}(\mathbf{r}) = V_{\max} e^{-2\kappa z}. \quad (2.5)$$

Its value at the surface $V_{\max} = d^2 E_0^2 / \hbar \Delta$ gives the maximum kinetic energy (in the z direction) of an atom that may be reflected at the barrier: $p_{zi}^2 / 2M \leq V_{\max}$. We suppose that the incident atomic velocity p_{zi} / M is sufficiently small that we may neglect tunneling effects and the van der Waals interaction with the surface compared to the optical potential. This is typically the case when the classical turning point distance from the surface

$$z_0 = \frac{1}{2\kappa} \ln \left(\frac{2MV_{\max}}{p_{zi}^2} \right) \quad (2.6)$$

is larger than about $\lambda_L / 2\pi$.

Since the optical potential of the evanescent wave has a simple exponential form (2.5), explicit analytical expressions for the classical trajectory and the quantum-mechanical wave function may be found [28–30]. More details are given in Appendix A.

III. THE LIGHT FIELD ABOVE THE ROUGH SURFACE

A. Result of the Rayleigh theory

Due to the roughness of the prism surface, the electric field above the surface contains a scattered part, in addition to the evanescent wave (2.3). We focus on surfaces with a rms surface roughness σ small compared to the optical wavelength, which is typically realized in experiments. The theory of light scattering at slightly rough surfaces may then be used to calculate the scattered part of the light field. In this section we recall the result one obtains for a scalar light field in the Rayleigh approximation, to first order in the surface roughness.

We only summarize this approach here; more details may be found in Refs. [22–27,31]. The scattered light field above and below the surface is expanded in Fourier components that are either propagating away from the surface or evanescent. The Fourier coefficients are determined by imposing, at the rough dielectric surface $z = s(\mathbf{R})$, the continuity relations for the total field (the field incident from below the surface plus the scattered field). The continuity relations are solved by iteration in ascending powers of the surface profile $s(\mathbf{R})$. At zeroth order, one finds the usual Fresnel transmission and reflection coefficients for the flat evanescent wave above the surface (2.3) and for the internally reflected field below the surface. To first order in the surface roughness, the scattered electric field is proportional to the transmitted zeroth-order field amplitude E_0 , the proportionality factor being typically of order $\kappa\sigma \ll 1$.

We write the Fourier expansion of the scattered field above the surface in the form

$$E^{(1)}(\mathbf{r}) = \int \frac{d^2 \mathbf{K}'}{(2\pi)^2} E^{(1)}(\mathbf{K}') \exp(i\mathbf{K}' \cdot \mathbf{R} - \kappa' z). \quad (3.1)$$

The scattered field modes are labeled by their in-plane wave vectors \mathbf{K}' and have decay constants κ' (either real and positive or imaginary with $\text{Im}\kappa' < 0$) given by

$$\kappa' = \sqrt{|\mathbf{K}'|^2 - k_L^2}. \quad (3.2)$$

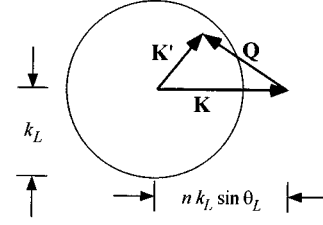


FIG. 2. Scattering of the light field by the rough surface. \mathbf{K}, \mathbf{K}' , in-plane wave vectors of the zeroth-order evanescent wave and the scattered light mode; \mathbf{Q} , in-plane wave vector of the surface roughness; circle, scattered wave vectors with $|\mathbf{K}'| = k_L$.

The Rayleigh approximation yields the following result for the Fourier coefficients of the scattered light, to first order in the surface roughness:

$$E^{(1)}(\mathbf{K}') = E_0 f(\mathbf{K}') \kappa S(\mathbf{K}' - \mathbf{K}). \quad (3.3)$$

They are proportional to the Fourier component $S(\mathbf{Q})$ of the surface profile $s(\mathbf{R})$,

$$S(\mathbf{Q}) = \int d^2 \mathbf{R} s(\mathbf{R}) e^{-i\mathbf{Q} \cdot \mathbf{R}}, \quad (3.4)$$

at the in-plane wave-vector transfer \mathbf{Q} between the scattered and the incident wave

$$\mathbf{Q} = \mathbf{K}' - \mathbf{K}. \quad (3.5)$$

The dimensionless factor $f(\mathbf{K}')$ in Eq. (3.3) is given by

$$f(\mathbf{K}') = \frac{i \sqrt{n^2 k_L^2 - |\mathbf{K}'|^2} + \kappa'}{\kappa}, \quad (3.6)$$

where the square root has to be taken with a positive imaginary part for $|\mathbf{K}'| > n k_L$.

Equation (3.5) shows that a specific Fourier component \mathbf{Q} of the surface roughness excites a scattered field mode with in-plane wave vector $\mathbf{K}' = \mathbf{K} + \mathbf{Q}$ from the incident wave (see Fig. 2). For a small wave-vector transfer \mathbf{Q} , the scattered mode is evanescent and the decay constant κ' is real. The wave-vector \mathbf{K}' is then located outside the circle in the figure. For larger wave vectors \mathbf{Q} [with magnitude at least equal to $k_L(n \sin \theta_L - 1)$], the scattered modes may be plane waves that propagate above the surface and \mathbf{K}' is then located inside the circle. In this case, the quantity κ' in the expansion (3.1) is imaginary with $\kappa' = -i k'_z$, where k'_z is the (real and positive) vertical component of the scattered wave vector.

B. Statistical model for the rough surface

We describe the roughness of the prism surface by a statistical approach and model the surface profile $s(\mathbf{R})$ by a random process. The mean surface height vanishes

$$\langle s(\mathbf{R}) \rangle = 0 \quad (3.7)$$

and its mean square is given by

$$\langle s^2(\mathbf{R}) \rangle = \sigma^2, \quad (3.8)$$

where σ is the rms surface roughness. We further assume that the surface roughness is statistically translation invariant, which means that the correlation function

$$\langle s(\mathbf{R}_1)s(\mathbf{R}_2) \rangle = C(\mathbf{R}_1 - \mathbf{R}_2) \quad (3.9)$$

depends only on the difference $\Delta \mathbf{R} \equiv \mathbf{R}_1 - \mathbf{R}_2$. The correlation function $C(\Delta \mathbf{R})$ is equal to σ^2 for $\Delta \mathbf{R} = \mathbf{0}$ and decreases to zero for $\Delta \mathbf{R} \rightarrow \infty$ on a scale equal to the correlation length l_S . We shall suppose that the surface roughness has Gaussian statistics, which means that its higher-order correlation functions are completely characterized by the average (3.7) and the correlation function (3.9).

For the Fourier transform $S(\mathbf{Q})$ of the surface profile, as defined in Eq. (3.4), Eqs. (3.7) and (3.9) yield the statistical averages

$$\langle S(\mathbf{Q}) \rangle = \langle S^*(\mathbf{Q}) \rangle = 0, \quad (3.10a)$$

$$\langle S(\mathbf{Q}_1)S^*(\mathbf{Q}_2) \rangle = (2\pi)^2 \mathcal{P}_S(\mathbf{Q}_1) \delta(\mathbf{Q}_1 - \mathbf{Q}_2). \quad (3.10b)$$

If the rough surface has a finite area A , the average (3.10b) becomes, for $\mathbf{Q}_1 = \mathbf{Q}_2$,

$$\langle S(\mathbf{Q})S^*(\mathbf{Q}) \rangle = A \mathcal{P}_S(\mathbf{Q}) \quad (3.10c)$$

and vanishes for $\mathbf{Q}_1 \neq \mathbf{Q}_2$. In Eqs. (3.10), $\mathcal{P}_S(\mathbf{Q})$ is the power spectrum of the surface roughness and it is equal to the Fourier transform of the correlation function $C(\Delta \mathbf{R})$. The width δQ_S of the power spectrum is related to the surface correlation length l_S by

$$\delta Q_S \sim \frac{1}{l_S}. \quad (3.11)$$

The rms surface roughness σ is obtained by integrating the power spectrum over all spatial frequencies

$$\sigma^2 = \int \frac{d^2 \mathbf{Q}}{(2\pi)^2} \mathcal{P}_S(\mathbf{Q}). \quad (3.12)$$

We note that an actual measurement of the rms roughness, with a surface scanning probe for example, involves only a limited range of spatial frequencies given by the bandwidth of the experimental device.

C. Validity of the light-scattering treatment

The validity domain of our calculation of the scattered light field is limited by two constraints. The first one arises from the use of the Rayleigh approximation. From numerical calculations of light scattering at periodic gratings, it has been found that this approximation is valid if the grating amplitude is small compared to the grating period [27]. In the context of rough surfaces, this condition becomes [31]

$$\sigma \ll l_S, \quad (3.13)$$

where l_S is the surface correlation length.

Another constraint comes from the fact that the scattered light amplitude is calculated only to first order in the surface roughness. This means that the rms surface roughness σ must be small compared to the wavelength of the incident and scattered light waves. For far-field calculations, the rel-

evant condition is $k_L \sigma \ll 1$ [27]. Since we are also interested in the light scattered into evanescent modes (with decay constant κ'), this condition has to be replaced by the somewhat stronger one that the rms roughness be small compared to the decay length of the scattered mode [32]

$$\sigma \ll 1/\kappa'. \quad (3.14)$$

A lower limit on $1/\kappa'$ is obtained from Eq. (3.2) and

$$\kappa' \approx |\mathbf{K}'| \approx |\mathbf{Q}| \quad (3.15)$$

for spatial frequencies \mathbf{K}', \mathbf{Q} large compared to k_L . If the roughness power spectrum has a width δQ_S much larger than the optical wave vector, evanescent modes with wave vectors up to $|\mathbf{K}'| \sim \delta Q_S$ are excited. In this case, the limits on the surface roughness σ imposed by the conditions (3.13) and (3.14) are of the same order of magnitude because the correlation length l_S is related to the width δQ_S of the power spectrum by Eq. (3.11). On the other hand, if the power spectrum is narrower than the optical wave vector, the correlation length l_S is larger than λ_L . In this case, $\kappa' \sim \kappa$ and condition (3.14) is more restrictive than Eq. (3.13).

In this paper we shall always suppose that the conditions (3.13) and (3.14) are satisfied. As far as the scattering of light at the rough surface is concerned, we may hence use the first-order perturbation theory outlined here.

IV. MODEL FOR THE ROUGH MIRROR POTENTIAL

We now calculate the optical potential of the evanescent wave mirror in the presence of light scattered at the rough dielectric surface. We therefore insert the total electric field and the unscattered and the scattered part [Eqs. (2.3) and (3.1)]

$$E(\mathbf{r}) = E^{(0)}(\mathbf{r}) + E^{(1)}(\mathbf{r}) \quad (4.1)$$

into the optical potential (2.1). Since the scattered field amplitude $E^{(1)}(\mathbf{r})$ is small compared to the unscattered field $E^{(0)}(\mathbf{r})$, the optical potential contains three terms of different orders of magnitude. To zeroth order in the surface roughness, we recover the flat optical potential $V^{(0)}(\mathbf{r})$ given in Eq. (2.5). The first-order potential $V^{(1)}(\mathbf{r})$ corresponds to the interference term between the scattered light field and the zeroth-order field. Finally, there is a second-order potential $V^{(2)}(\mathbf{r})$ proportional to the square of $E^{(1)}(\mathbf{r})$. Close to the surface (at distances of order $1/\kappa$), this second-order term is small compared to the first-order potential $V^{(1)}(\mathbf{r})$. On the other hand, it is nonzero in the half space above the surface because of the propagating modes in the scattered light field. As mentioned in the Introduction, we focus in this paper on the roughness of the optical potential around the point where the atoms are reflected and ignore the potential $V^{(2)}(\mathbf{r})$.

In our model, the roughness of the evanescent wave mirror is therefore described by the optical potential

$$V^{(1)}(\mathbf{r}) = \frac{d^2}{\hbar \Delta} [E^{(0)*}(\mathbf{r})E^{(1)}(\mathbf{r}) + E^{(1)*}(\mathbf{r})E^{(0)}(\mathbf{r})], \quad (4.2)$$

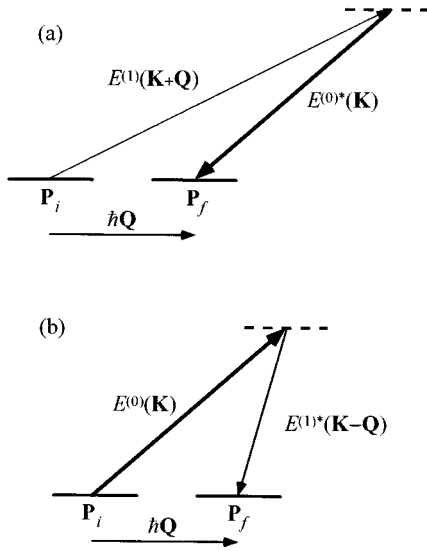


FIG. 3. Interpretation of the atomic scattering in terms of Raman transitions involving absorption and stimulated emission.

which is created by the interference between the flat evanescent wave $E^{(0)}(\mathbf{r})$ and the light scattered at the rough surface $E^{(1)}(\mathbf{r})$ [33]. Using the expansion (3.1) of the scattered light field $E^{(1)}(\mathbf{r})$, we represent the rough potential (4.2) as a two-dimensional Fourier integral

$$V^{(1)}(\mathbf{r}) = \int \frac{d^2\mathbf{Q}}{(2\pi)^2} \tilde{V}^{(1)}(\mathbf{Q}, z) e^{i\mathbf{Q}\cdot\mathbf{R}}, \quad (4.3)$$

with

$$\begin{aligned} \tilde{V}^{(1)}(\mathbf{Q}, z) = & V_{\max} \kappa S(\mathbf{Q}) \{ f(\mathbf{K} + \mathbf{Q}) \exp[-(\kappa + \kappa'_+)z] \\ & + f^*(\mathbf{K} - \mathbf{Q}) \exp[-(\kappa + \kappa'_-)z] \}. \end{aligned} \quad (4.4)$$

The functions $f(\mathbf{K} \pm \mathbf{Q})$ defined in Eq. (3.6) provide the amplitudes of the scattered light modes with the in-plane wave vectors $\mathbf{K} \pm \mathbf{Q}$. The κ'_\pm are the decay (or propagation) constants of these modes.

We note that the Fourier transform $\tilde{V}^{(1)}(\mathbf{Q}, z)$ of the rough potential is proportional to the Fourier amplitude $S(\mathbf{Q})$ of the surface roughness. The spatial frequencies of the rough potential are therefore the same as those of the rough surface. However, a given Fourier component of the surface roughness contributes to the rough potential via two scattered light modes with the in-plane wave vectors $\mathbf{K} \pm \mathbf{Q}$.

We may interpret these contributions in terms of two Raman transitions that both transfer an in-plane momentum $\Delta\mathbf{P} = \hbar\mathbf{Q}$ to the atom. These transitions are schematized in Fig. 3. In the first Raman transition [Fig. 3(a)], the atom absorbs a photon from a scattered light mode with wave vector $\mathbf{K} + \mathbf{Q}$ and subsequently emits another one into the zeroth-order evanescent wave. The atomic in-plane momentum transfer for this stimulated Raman process is

$$\Delta\mathbf{P} = \hbar(\mathbf{K} + \mathbf{Q}) - \hbar\mathbf{K}. \quad (4.5)$$

Its transition amplitude is proportional to [cf. Eq. (3.3)]

$$E_0^* E^{(1)}(\mathbf{K} + \mathbf{Q}) = \kappa S(\mathbf{Q}) f(\mathbf{K} + \mathbf{Q}) |E_0|^2 \quad (4.6)$$

and corresponds to the first term in Eq. (4.4). In the second Raman transition [Fig. 3(b)], a photon from the zeroth-order field is absorbed and another one emitted into a scattered light mode with wave vector $\mathbf{K} - \mathbf{Q}$, leading to the atomic momentum transfer

$$\Delta\mathbf{P} = \hbar\mathbf{K} - \hbar(\mathbf{K} - \mathbf{Q}). \quad (4.7)$$

The Raman transition amplitude is proportional to [cf. the second term in Eq. (4.4)]

$$E^{(1)*}(\mathbf{K} - \mathbf{Q}) E_0 = \kappa S^*(-\mathbf{Q}) f^*(\mathbf{K} - \mathbf{Q}) |E_0|^2. \quad (4.8)$$

As a consequence of the relation $S^*(-\mathbf{Q}) = S(\mathbf{Q})$ [which follows from Eq. (3.4)], the relative phase of the transition amplitudes (4.6) and (4.8) is independent of the (random) phase of the Fourier coefficient $S(\mathbf{Q})$. For a given wave vector \mathbf{Q} of the surface roughness, the two Raman processes therefore add up coherently in the rough dipole potential.

V. DIFFUSE ATOMIC REFLECTION IN THE BORN APPROXIMATION

In this section we use potential scattering theory in the Born approximation to characterize the diffuse reflection of an atomic wave at the evanescent wave mirror. Our treatment is equivalent to the distorted-wave Born approximation, applied, e.g., in atomic collision theory, and we compute the transition probabilities among the exact eigenstates in the flat mirror potential. We define an average differential probability of diffuse reflection by means of the scattering cross section for the rough optical potential $V^{(1)}(\mathbf{r})$. This differential probability gives the distribution of the in-plane momentum transfer for the diffusely reflected atoms. We discuss and analyze this momentum transfer and the total probability of diffuse reflection. Finally, we estimate the validity of the Born approximation.

A. Average differential probability of diffuse reflection in the Born approximation

Consider an atomic wave that is incident upon the evanescent wave mirror with momentum $\mathbf{p}_i = (\mathbf{P}_i, -p_{zi})$, at an angle of incidence θ_i with respect to the mean surface normal (cf. Fig. 1). If the mirror potential has no roughness, the atomic wave is specularly reflected and its wave function is given by an eigenfunction of the flat potential (2.5)

$$\phi_i(\mathbf{r}) = \exp(i\mathbf{P}_i \cdot \mathbf{R}/\hbar) \phi_{p_{zi}}(z). \quad (5.1)$$

The z -dependent part of the wave function $\phi_{p_{zi}}(z)$ is given in Appendix A. Far from the mirror surface, it is the sum of an incident and a reflected wave with momenta $\mp p_{zi}$. We choose the normalization

$$\phi_{p_{zi}}(z) = \sin(p_{zi}z/\hbar + \varphi), \quad z \rightarrow \infty, \quad (5.2)$$

where φ is a phase shift that depends on the incident momentum and the magnitude V_{\max} of the zeroth-order potential [30].

From the point of view of scattering theory, the rough part $V^{(1)}(\mathbf{r})$ of the mirror potential induces transitions from the initial state $\psi_i(\mathbf{r})$ into a final state $\psi_f(\mathbf{r})$ with momentum

$\mathbf{p}_f = (\mathbf{P}_f, p_{zf})$. Since the rough potential is time independent, energy conservation implies that

$$\mathbf{P}_f^2 + p_{zf}^2 = \mathbf{P}_i^2 + p_{zi}^2. \quad (5.3)$$

In the first Born approximation, the differential cross section for this transition is given by

$$\begin{aligned} \frac{d\Sigma}{d\Omega_f} &= \frac{4M^2}{\pi^2 \hbar^4} |\langle \psi_f(\mathbf{r}) | V^{(1)}(\mathbf{r}) | \psi_i(\mathbf{r}) \rangle|^2 \\ &= \frac{4M^2}{\pi^2 \hbar^4} |\langle \phi_{p_{zf}}(z) | \tilde{V}^{(1)}(\mathbf{Q}, z) | \phi_{p_{zi}}(z) \rangle|^2, \end{aligned} \quad (5.4)$$

where M is the atomic mass and $d\Omega_f$ the element of solid angle around \mathbf{p}_f . The prefactor of the scattering cross section (5.4) is explained by our particular choice of normalization for the atomic wave functions (see Appendix A). By an appropriate normalization of the scattering cross section, as given in Appendix A, we obtain a differential probability of diffuse reflection per in-plane wave-vector transfer \mathbf{Q} :

$$\frac{dw}{d\mathbf{Q}} = \frac{\hbar^2}{p_{zi} p_{zf} A} \frac{1}{d\Omega_f}, \quad (5.5)$$

where A is the mirror surface area.

This is the diffuse reflection probability for a particular realization of the rough dielectric surface. In the framework of our statistical approach, we calculate its average value with respect to the statistical ensemble (3.10). We expect that the ensemble average equals the average over a large number of reflected atoms from a single realization of the rough surface, if the atoms are reflected independently and sample uncorrelated parts of the surface.

B. Calculation of the diffuse reflection probability

From the Born cross section (5.4) and the Fourier component of the rough potential (4.4), we find that the average cross section $\langle d\Sigma/d\Omega_f \rangle$ is proportional to $\langle S(\mathbf{Q})S^*(\mathbf{Q}) \rangle$. Since this quantity is proportional to the area A [cf. Eq. (3.10c)], the finite mirror surface drops out of the average diffuse reflection probability (5.5). The latter is then obtained as a simple product of the surface power spectrum and an ‘‘atomic response function’’

$$\left\langle \frac{dw}{d\mathbf{Q}} \right\rangle = (2\pi)^{-2} \mathcal{P}_S(\mathbf{Q}) |B_{\text{at}}(\mathbf{Q})|^2, \quad (5.6)$$

where $B_{\text{at}}(\mathbf{Q})$ is given by

$$\begin{aligned} B_{\text{at}}(\mathbf{Q}) &= \frac{4M\kappa}{\hbar} \frac{V_{\text{max}}}{\sqrt{p_{zi} p_{zf}}} \\ &\times \langle \phi_{p_{zf}}(z) | \{ f(\mathbf{K} + \mathbf{Q}) \exp[-(\kappa + \kappa'_+)z] \\ &+ f^*(\mathbf{K} - \mathbf{Q}) \exp[-(\kappa + \kappa'_-)z] \} | \phi_{p_{zi}}(z) \rangle. \end{aligned} \quad (5.7)$$

This function characterizes the diffuse atomic reflection for a given spatial frequency in the surface roughness.

To calculate the diffuse reflection probability, we are now left with the matrix element

$$\langle \phi_{p_{zf}}(z) | \exp[-(\kappa + \kappa')z] | \phi_{p_{zi}}(z) \rangle, \quad (5.8)$$

which describes the coupling between the initial and final atomic states due to the rough potential. In the first Born approximation of potential scattering, it is known that the momentum change is distributed according to the Fourier transform of the potential and we expect that the exponential decay of the field limits the normal momentum change by

$$|\Delta p_z| \equiv |p_{zf} - p_{zi}| \lesssim \hbar \kappa. \quad (5.9)$$

The integral (5.8) can actually be done analytically and is given in Appendix A. We shall concentrate on the semiclassical limit where the atomic de Broglie wavelength is small compared to the decay length of the potential. This regime corresponds to an incident momentum with

$$p_{zi} \gg \hbar \kappa, \quad (5.10)$$

and in this limit, the matrix element can be written in the form

$$\begin{aligned} &\langle \phi_{p_{zf}}(z) | \exp[-(\kappa + \kappa')z] | \phi_{p_{zi}}(z) \rangle \\ &= (2\kappa)^{-1} \exp[-(\kappa + \kappa')z_0] \sqrt{\frac{p_{zf}}{p_{zi}} \left(\frac{p_{zf} + p_{zi}}{2p_{zi}} \right)^{\kappa'/\kappa}} \\ &\times \beta \left(\frac{\Delta p_z}{\hbar \kappa}, \frac{\kappa'}{\kappa} \right), \end{aligned} \quad (5.11)$$

where z_0 is the classical turning point for the incident velocity p_{zi}/M in the flat mirror potential.

The dimensionless function β is defined by

$$\begin{aligned} \beta \left(\frac{\Delta p_z}{\hbar \kappa}, \frac{\kappa'}{\kappa} \right) &= \frac{2^{\kappa'/\kappa}}{2 \Gamma[(\kappa + \kappa')/\kappa]} \Gamma \left(\frac{\kappa + \kappa'}{2\kappa} + i \frac{\Delta p_z}{2\hbar \kappa} \right) \\ &\times \Gamma \left(\frac{\kappa + \kappa'}{2\kappa} - i \frac{\Delta p_z}{2\hbar \kappa} \right), \end{aligned} \quad (5.12)$$

where Γ is the Euler gamma function. We shall call β the ‘‘overlap factor.’’ It is real (complex) valued for real (imaginary) κ' . One has the explicit expressions [34]

$$\beta \left(\frac{\Delta p_z}{\hbar \kappa}, 1 \right) = \frac{\pi \Delta p_z / 2\hbar \kappa}{\sinh(\pi \Delta p_z / 2\hbar \kappa)} \quad \text{for } \kappa' = \kappa, \quad (5.13a)$$

$$\beta \left(\frac{\Delta p_z}{\hbar \kappa}, 0 \right) = \frac{\pi/2}{\cosh(\pi \Delta p_z / 2\hbar \kappa)} \quad \text{for } \kappa' = 0. \quad (5.13b)$$

They show that the overlap factor takes its maximum value for $\Delta p_z = 0$ and decreases exponentially if Δp_z is large compared to $\hbar \kappa$, which is in agreement with our expectation (5.9) that the normal atomic momentum change is limited to $\hbar \kappa$. This cutoff implies that we may make the following approximation in the matrix element (5.11):

$$\sqrt{\frac{p_{zf}}{p_{zi}} \left(\frac{p_{zf} + p_{zi}}{2p_{zi}} \right)^{\kappa'/\kappa}} \approx 1, \quad (5.14)$$

neglecting corrections of relative order $|\Delta p_z|/p_{zi} \lesssim \hbar \kappa/p_{zi}$, which are small in the semiclassical regime (5.10). To the same approximation, we may also replace the square root $\sqrt{p_{zi} p_{zf}}$ by p_{zi} in Eq. (5.7). If we finally express the height V_{\max} of the zeroth-order potential in terms of the turning point z_0 [Eq. (2.6)], we obtain the following result for the atomic response function (5.7):

$$B_{\text{at}}(\mathbf{Q}) = \frac{p_{zi}}{\hbar} \{ f(\mathbf{K} + \mathbf{Q}) \exp[(\kappa - \kappa'_+)z_0] \beta_+ + f^*(\mathbf{K} - \mathbf{Q}) \exp[(\kappa - \kappa'_-)z_0] \beta_-^* \}, \quad (5.15)$$

where β_{\pm} is a shorthand notation for the overlap factors $\beta(\Delta p_z/\hbar \kappa, \kappa'_{\pm}/\kappa)$.

C. Discussion of the diffuse reflection probability

1. Shape of the atomic response function

We discuss in this subsection the behavior of the differential diffuse reflection probability $\langle dw/d\mathbf{Q} \rangle$ as a function of the in-plane atomic momentum transfer $\Delta \mathbf{P} = \hbar \mathbf{Q}$. According to Eq. (5.6), the maximum first-order momentum transfer δP_{Born} is determined by both the width δQ_S of the roughness power spectrum $\mathcal{P}_S(\mathbf{Q})$ and the width δQ_{at} of the atomic response function $B_{\text{at}}(\mathbf{Q})$.

In order to determine the width δQ_{at} of the atomic response function, we observe three features of the result (5.15): (a) the ‘‘optical response function’’ $f(\mathbf{K} \pm \mathbf{Q})$, which characterizes the scattering of the light field by a given spatial frequency of the rough surface [cf. Eq. (3.3)]; (b) the amplitude $\exp(-\kappa'_{\pm} z_0)$ of the scattered light modes at the distance z_0 of the atomic turning point [cf. Eq. (3.1)]; and (c) the overlap factor $\beta(\Delta p_z/\hbar \kappa, \kappa'_{\pm}/\kappa)$, which characterizes the coupling between the initial and final atomic wave functions induced by the rough potential [cf. Eq. (5.11)].

(a) *Optical response function.* The absolute value of $f(\mathbf{K}')$ is represented in Fig. 4(a), as a function of the magnitude $|\mathbf{K}'|$ of the scattered wave vector. We see that the optical response function is of the order of unity for $|\mathbf{K}'| \lesssim n k_L$ and decreases proportional to $1/|\mathbf{K}'|$ for larger wave vectors (the dashed line). It therefore introduces a smooth cutoff for high spatial frequencies in the scattered light.

(b) *Distance of the atomic turning point.* Figure 4(b) shows the absolute value of the light field amplitude $\exp(-\kappa' z_0)$ as a function of $|\mathbf{K}'|$, for different values of the turning point distance z_0 . We see that for a turning point rather close to the surface (the thick solid line), the amplitudes of the scattered light field are comparable for propagating ($|\mathbf{K}'| < k_L$) and evanescent ($|\mathbf{K}'| > k_L$) modes. Figure 5 represents the square of the atomic response function (5.15) for this turning point distance ($z_0 = \frac{1}{2} \kappa^{-1} \ln 2$). In this figure the atoms are reflected at normal incidence. The response function has a quite complex shape, but we see that spatial frequencies much larger than the optical wave vector do not contribute to the diffuse reflection.

The atomic response function becomes somewhat simpler if the turning point distance z_0 is larger. The dashed line in Fig. 4(b) (for $z_0 = 2 \kappa^{-1} \ln 2$) then shows that the amplitudes of evanescent modes are small and only propagating modes

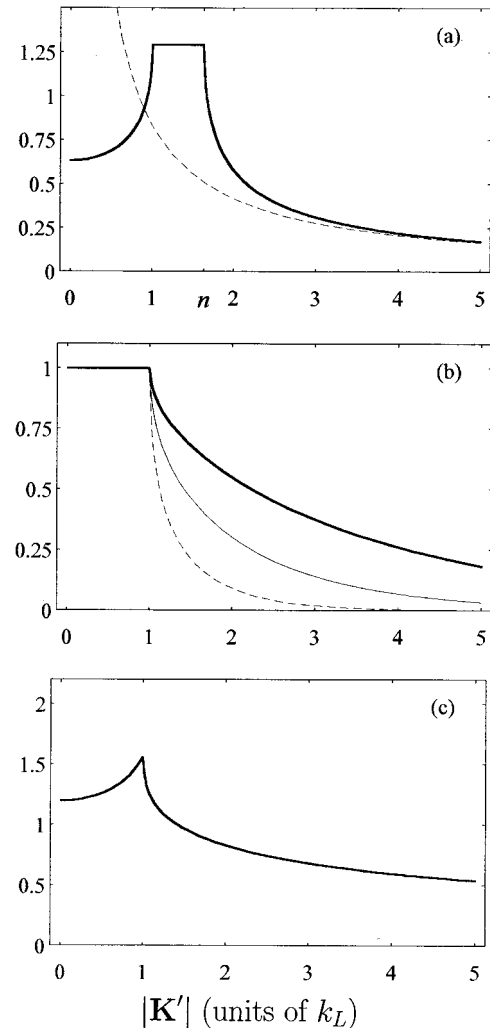


FIG. 4. (a) Absolute value of the optical response function $f(\mathbf{K}')$ (3.6), as a function of the magnitude of the scattered optical wave vector \mathbf{K}' (in units of the vacuum wave vector k_L). The dashed curve gives the asymptotic behavior inversely proportional to $|\mathbf{K}'|$ for large $|\mathbf{K}'|$. The refractive index equals $n \approx 1.63$ and $\kappa = k_L$. (b) Absolute value of the field amplitude $\exp(-\kappa' z_0)$, as a function of $|\mathbf{K}'|$. Thick solid line, turning point rather close to the surface $z_0 = \frac{1}{2} \kappa^{-1} \ln 2$; thin solid line, intermediate distance $z_0 = \kappa^{-1} \ln 2$; dashed line, large distance $z_0 = 2 \kappa^{-1} \ln 2$. (c) Absolute value of the overlap factor β (5.12), as a function of $|\mathbf{K}'|$. The normal momentum difference is $\Delta p_z = 0$; this situation is approximately realized at normal atomic incidence.

contribute to the rough potential. The corresponding atomic response function is represented in Fig. 6. Its dominant features are two disks of radius k_L and centered at $\pm \mathbf{K}$. For these spatial frequencies, the diffuse reflection is due to propagating light modes: in terms of the Raman transitions of Fig. 3, the left disk corresponds to the transition of Fig. 3(a), where the absorbed photon with wave vector $\mathbf{K}' = \mathbf{K} + \mathbf{Q}$ is propagating ($|\mathbf{K}'| < k_L$). The disk is centered at $-\mathbf{K}$ because of the recoil from the photon emission into the zeroth-order evanescent wave. The right disk corresponds to the transition of Fig. 3(b), where the emitted photon (wave vector $\mathbf{K}' = \mathbf{K} - \mathbf{Q}$) is propagating. Note the anisotropy of the atomic response function: it is broader parallel to the propagation vector \mathbf{K} of the zeroth-order evanescent wave.

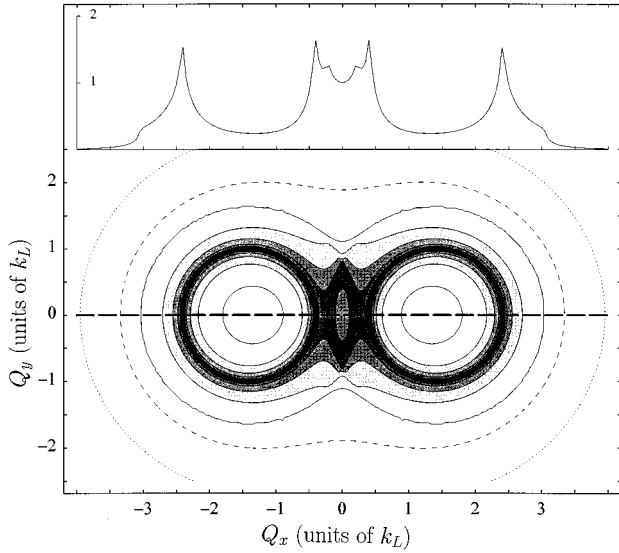


FIG. 5. Contour plot of the atomic response function $|B_{\text{at}}(\mathbf{Q})|^2$ (5.15) at normal incidence, as a function of the atomic in-plane wave-vector transfer \mathbf{Q} in units of the optical wave vector k_L . Shaded areas correspond to large values of the response function. The inset shows a profile along the thick dashed line. The turning point is close to the surface $z_0 = \frac{1}{2}\kappa^{-1}\ln 2$ and atoms are incident with normal momentum $p_{zi} = 50\hbar\kappa$. The zeroth-order evanescent wave has an in-plane wave vector $\mathbf{K} = \sqrt{2} k_L \mathbf{e}_x$ parallel to the x axis and $\kappa = k_L$.

(c) *Role of the overlap factor.* We recall that the overlap factor β limits the normal momentum difference to $|\Delta p_z| \leq \hbar\kappa$ [cf. Eq. (5.13)]. At normal atomic incidence, this does not impose a significant restriction on the width of the atomic response function because the normal momentum changes only to second order in the in-plane momentum transfer $\hbar\mathbf{Q}$: from Eqs. (5.3) and (5.9), we find the limit $\delta Q_{\text{at}} \lesssim \sqrt{2} p_{zi} \kappa / \hbar$, which, in the semiclassical regime, is typi-

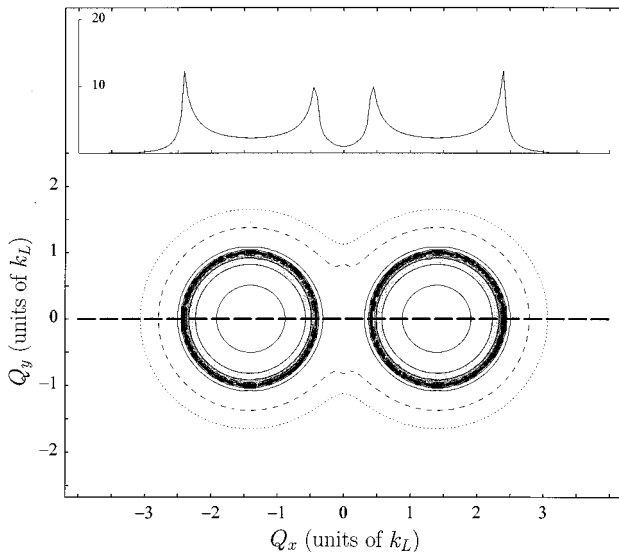


FIG. 6. Same as Fig. 5, but with an increased optical potential such that the turning point is farther away from the surface: $z_0 = 2\kappa^{-1}\ln 2$.

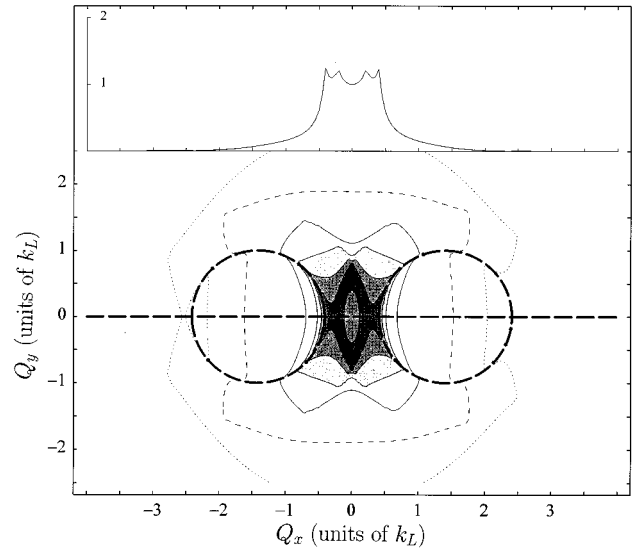


FIG. 7. Same as Fig. 5, but at oblique incidence: $\theta_i = 45^\circ$ with normal momentum component $p_{zi} = 50\hbar\kappa$. The atoms are incident in the same plane as the light beam creating the evanescent wave (the x - z plane) with $\mathbf{P}_i = 50\hbar\kappa \mathbf{e}_x$. Inside the dashed circles, propagating light modes contribute to the diffuse atomic reflection.

cally large compared to the size of the double disk structure discussed above.

At oblique incidence, however, the normal atomic momentum changes to first order in $\hbar\mathbf{Q}$ because of energy conservation. Parallel to the incident in-plane momentum \mathbf{P}_i , the overlap factor then limits the width of the response function to spatial frequencies $\delta Q_{\text{at}} \lesssim \kappa / \tan \theta_i$, where θ_i is the atomic angle of incidence. This is a significant restriction because it is of the order of the optical wave vector. Perpendicular to the atomic plane of incidence, the limit for δQ_{at} is large compared to k_L , similar to the case of normal incidence. This implies that if the atoms are incident at a grazing angle ($\theta_i \rightarrow 90^\circ$, but p_{zi} still large compared to $\hbar\kappa$), the diffuse reflection is strongly suppressed in the atomic plane of incidence. For a sufficiently broad surface power spectrum $\mathcal{P}_S(\mathbf{Q})$, the angular distribution of the reflected atoms should therefore be broader in the direction perpendicular to the atomic plane of incidence.

In Figs. 7 and 8 we show the atomic response function for atoms incident at an angle $\theta_i = 45^\circ$ for two different experimental situations. (The turning point is located at $z_0 = \frac{1}{2}\kappa^{-1}\ln 2$, as in Fig. 5.) In Fig. 7 the atomic and optical planes of incidence coincide (incident atomic momentum \mathbf{P}_i parallel to the propagation vector \mathbf{K} of the zeroth-order evanescent wave). In this geometry, the atomic response function is flattened in the direction parallel to \mathbf{K} and its anisotropy is reduced. In Fig. 8 \mathbf{P}_i and \mathbf{K} are perpendicular and the anisotropy of the response function is increased.

Finally, we recall that the overlap factor β also varies with the decay constants κ'_\pm of the scattered light modes. Its absolute value is shown in Fig. 4(c) for $\Delta p_z = 0$, as a function of $|\mathbf{K}'|$. The coupling between the atomic wave functions is peaked at $|\mathbf{K}'| = k_L$ because the scattered light modes are then constant above the surface ($\kappa'_\pm = 0$). The coupling is smaller both for propagating and evanescent modes. For propagating modes, this is due to the averaging over the

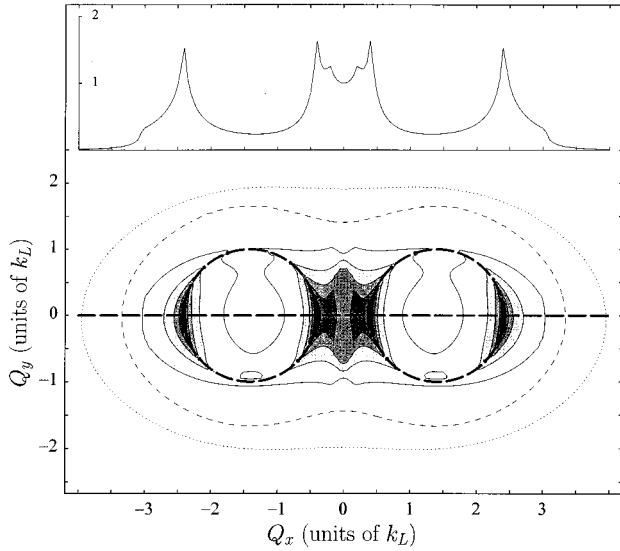


FIG. 8. Same as Fig. 7, the optical plane of incidence (the x - z plane) being perpendicular to the atomic plane of incidence (the y - z plane) with $\mathbf{P}_i = 50\hbar \kappa \mathbf{e}_y$.

oscillating field amplitude in the matrix element (5.8). This behavior of the overlap factor enhances the atomic response function on the perimeters of the two circles identified above, which is apparent in Figs. 5 and 6 (cf. also the inset of Fig. 5, showing a profile of the response function squared along the dashed horizontal line). At oblique incidence (Figs. 7 and 8), the enhancement is less visible because of the stronger variation of the momentum difference Δp_z .

Summarizing, the width δQ_{at} of the atomic response function $B_{\text{at}}(\mathbf{Q})$ is of the order of a few optical wave vectors. Its detailed shape depends on the distance of the turning point as well as on the geometry of incidence.

2. Order of magnitude of the diffuse reflection probability

We find the total (first-order) probability of diffuse reflection w by integrating the differential probability (5.6) over all spatial frequencies:

$$w = \int d^2\mathbf{Q} \left\langle \frac{dw}{d\mathbf{Q}} \right\rangle = \int \frac{d^2\mathbf{Q}}{(2\pi)^2} \mathcal{P}_S(\mathbf{Q}) |B_{\text{at}}(\mathbf{Q})|^2. \quad (5.16)$$

The form (5.15) of the atomic response function $B_{\text{at}}(\mathbf{Q})$ suggests that we may define an ‘‘effective roughness’’ $\sigma_{\text{eff}}(\theta_i, z_0)$ for the atomic mirror by the integral

$$\begin{aligned} \sigma_{\text{eff}}^2(\theta_i, z_0) &\equiv \frac{1}{4} \int \frac{d^2\mathbf{Q}}{(2\pi)^2} \mathcal{P}_S(\mathbf{Q}) |f(\mathbf{K} + \mathbf{Q}) \\ &\quad \times \exp[(\kappa - \kappa'_+)z_0] \beta_+ + f^*(\mathbf{K} - \mathbf{Q}) \\ &\quad \times \exp[(\kappa - \kappa'_-)z_0] \beta_-^*|^2, \end{aligned} \quad (5.17)$$

where the power spectrum of the rough surface is weighted by a factor proportional to the square of the atomic response function. As discussed in Sec. V C 1, spatial frequencies up to a few optical wave vectors contribute to the effective roughness (5.17). The probability of diffuse reflection (5.16) may now be written in the standard form

$$w = [2p_{z_i} \sigma_{\text{eff}}(\theta_i, z_0) / \hbar]^2 = \left(\frac{4\pi \cos\theta_i \sigma_{\text{eff}}(\theta_i, z_0)}{\lambda_{\text{dB}}} \right)^2, \quad (5.18)$$

where $\lambda_{\text{dB}} = 2\pi\hbar/|\mathbf{p}_i|$ is the de Broglie wavelength of the incident atoms. This result shows that the atomic reflection at the evanescent wave mirror is specular only if the effective roughness is smaller than the atomic wavelength.

In order to give a more physical interpretation of the quantity $\sigma_{\text{eff}}(\theta_i, z_0)$, we introduce the turning point surface $z_0(\mathbf{R})$, where the value of the optical potential is equal to the incident energy. We note that since the optical potential is proportional to the optical near field intensity, the turning point surface is a particular iso-intensity surface and may be obtained experimentally by optical near-field microscopy [35–37].

In the absence of roughness, the turning point surface $z_0(\mathbf{R})$ is flat and located at the turning point z_0 . In the presence of the small rough potential $V^{(1)}(\mathbf{r})$, it acquires some roughness and its deviation from the mean position is approximately given by [cf. Eq. (2.6)]

$$\delta z_0(\mathbf{R}) \approx \frac{1}{2\kappa} \frac{V^{(1)}(\mathbf{R}, z_0)}{V^{(0)}(z_0)}. \quad (5.19)$$

We may now describe the rough evanescent wave mirror by an infinite potential barrier located at the rough turning point surface. This model is known as the corrugated hard wall potential and is used in the scattering of atoms from crystalline surfaces [14–16]. In the Rayleigh approximation and for $\delta z_0(\mathbf{R})$ small compared to the atomic wavelength, one may show that this model gives a total diffuse reflection probability of the same form as Eq. (5.18). Assuming small scattering angles, the effective roughness of the atomic mirror is given by the rms roughness σ_{z_0} of the turning point surface:

$$\begin{aligned} \sigma_{z_0}^2 &\equiv \langle [\delta z_0(\mathbf{R})]^2 \rangle \\ &= \frac{1}{4} \int \frac{d^2\mathbf{Q}}{(2\pi)^2} \mathcal{P}_S(\mathbf{Q}) |f(\mathbf{K} + \mathbf{Q}) \exp[(\kappa - \kappa'_+)z_0] \\ &\quad + f^*(\mathbf{K} - \mathbf{Q}) \exp[(\kappa - \kappa'_-)z_0]|^2. \end{aligned} \quad (5.20)$$

Comparing this expression to the effective roughness (5.17), we observe that the corrugated hard wall potential does not reproduce the overlap factors β_{\pm} . The difference between $\sigma_{\text{eff}}(\theta_i, z_0)$ and σ_{z_0} is small, however, if the variation of the overlap factor $\beta(\Delta p_z / \hbar \kappa, \kappa' / \kappa)$ is negligible in the range of spatial frequencies that contribute to the integral (5.20). We recall that this is the case at normal incidence because the normal momentum change Δp_z is small and β depends weakly on κ' , as already shown in Fig. 4(c).

The concept of the rough turning point surface also allows us to understand the dependence of the effective roughness $\sigma_{\text{eff}}(\theta_i, z_0)$ on the turning point distance z_0 . According to Eq. (5.19), the roughness of the surface $z_0(\mathbf{R})$ is determined by the relative variation of the optical potential at the distance z_0 . Scattered light modes that decay more slowly than the zeroth-order evanescent wave ($\kappa'_\pm < \kappa$) and propagating modes (κ'_\pm imaginary) therefore give contributions to $\sigma_{\text{eff}}(\theta_i, z_0)$ and σ_{z_0} that increase with z_0 [cf. Eqs. (5.20) and

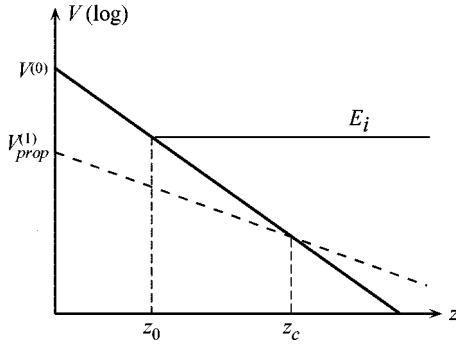


FIG. 9. Zeroth- and first-order optical potentials in logarithmic scale. Solid line, zeroth-order optical potential $V^{(0)}(z)$ (2.5), with z_0 the classical turning point; dashed line, optical potential $V_{\text{prop}}^{(1)}(z)$ (5.22) created by the interference of a propagating scattered light mode with the zeroth-order evanescent wave.

(5.20)]. This observation yields a simple estimate for $\sigma_{\text{eff}}(\theta_i, z_0)$: the factor weighting the surface power spectrum in Eq. (5.17) is maximum for propagating light modes, where it is of order $e^{2\kappa z_0}$. The effective roughness is therefore overestimated by $\sigma_{\text{eff}}(\theta_i, z_0) \approx \sigma e^{\kappa z_0}$. We then find the following upper limit for the total diffuse reflection probability (5.18):

$$w \lesssim \left(\frac{4\pi \cos \theta_i \sigma e^{\kappa z_0}}{\lambda_{\text{dB}}} \right)^2. \quad (5.21)$$

The atomic reflection at the evanescent wave mirror is therefore specular only if the rms roughness σ of the dielectric surface itself is smaller than the wavelength of the incident atoms. Furthermore, if one pushes the turning point z_0 farther away from the surface, by using an optical potential V_{max} much larger than the incident kinetic energy $E_i = p_{z_i}^2/2M$, the diffuse reflection probability increases by a factor $e^{2\kappa z_0} = V_{\text{max}}/E_i$.

Finally, at oblique incidence, the range of wave vectors that contribute to the effective roughness $\sigma_{\text{eff}}(\theta_i, z_0)$ (5.17) is smaller due to the narrowing of the atomic response function, as shown in Figs. 7 and 8. As a consequence, the diffuse reflection probability is below the estimate (5.21).

D. Validity of the Born approximation

We recall that we describe the rough optical potential $V^{(1)}(\mathbf{r})$ of the evanescent wave mirror by perturbation theory. We have seen that for a broad surface power spectrum, the dominant contribution to this potential comes from propagating light modes: the corresponding optical potential $V_{\text{prop}}^{(1)}(\mathbf{r})$ is of the order of

$$V_{\text{prop}}^{(1)}(\mathbf{r}) \approx \kappa \sigma V_{\text{max}} e^{-\kappa z} \quad (5.22)$$

and crosses the zeroth-order potential at a distance z_c given by

$$\kappa \sigma \approx e^{-\kappa z_c}. \quad (5.23)$$

This is illustrated in Fig. 9. A necessary condition for the perturbation theory to be valid is that the zeroth-order potential $V^{(0)}(z)$ (close to the surface) and the incident normal

kinetic energy E_i (far from the surface) be larger than $V_{\text{prop}}^{(1)}(\mathbf{r})$. As can be seen from Fig. 9, this condition is equivalent to the requirement that the crossing point z_c be farther from the surface than the turning point z_0 . In terms of the surface roughness σ , this yields the condition

$$\sigma \ll \frac{e^{-\kappa z_0}}{\kappa}. \quad (5.24)$$

We note that this condition is satisfied if the optical perturbation theory for the light scattering at the rough surface is valid [cf. Eq. (3.14)].

In addition, we must verify that the Born approximation for the diffuse atomic reflection is justified, i.e., that we are in the quasispecular regime ($w \ll 1$). According to Eq. (5.18), this regime is characterized by an effective surface roughness $\sigma_{\text{eff}}(\theta_i, z_0)$ small compared to the incident atomic wavelength. At normal incidence, we may use the estimate (5.21) for the diffuse reflection probability to find the more practical formulation

$$\sigma \ll \frac{\lambda_{\text{dB}}}{4\pi \cos \theta_i} e^{-\kappa z_0}. \quad (5.25)$$

This condition requires the surface roughness σ to be below the incident atomic wavelength λ_{dB} , which is a more severe restriction than Eq. (5.24). At oblique incidence, the diffuse reflection probability is smaller than the estimate (5.21) and the Born approximation remains valid even if the surface roughness σ surpasses the limit (5.25).

VI. DIFFUSE ATOMIC REFLECTION IN THE THIN PHASE GRATING APPROXIMATION

We now present a calculation of the momentum distribution of the diffusely reflected atoms that is able to go beyond the Born approximation. The rough optical potential of the evanescent wave mirror is taken into account by a phase shift of the reflected atomic wave, in a way similar to a phase grating in conventional optics. The phase-shifted wave function allows us to compute the spatial coherence function of the reflected atoms. The coherence function gives the (average) momentum distribution by means of a Fourier transform.

We show that this approach recovers the Born approximation in the quasispecular regime and study then the diffuse regime where the surface roughness is larger than the atomic wavelength. For a large decay length $1/\kappa$, however, the evanescent wave realizes a thick grating for the atoms and the thin phase grating approximation becomes invalid, whereas the Born approximation may still apply, provided the reflection is quasispecular. In addition, we recall that the thin phase grating approach is a semiclassical method and we are therefore truly limited to the regime (5.10).

A. Principle of the calculation

The central idea of the thin phase grating approach is that the diffuse reflection from the rough mirror distorts the wave front of the atomic matter wave. At a fixed position $(\mathbf{R}, z=h)$ above the mirror, we therefore write the reflected wave function $\psi_r(\mathbf{R})$ in the form

$$\psi_r(\mathbf{R}) = \psi_r^{(0)}(\mathbf{R}) \exp[i \delta\varphi(\mathbf{R})], \quad (6.1)$$

where $\psi_r^{(0)}(\mathbf{R})$ is the wave function reflected at the flat mirror and $\delta\varphi(\mathbf{R})$ its phase shift. The height h is kept fixed and is suppressed to simplify the notation.

We shall place ourselves in the semiclassical regime where the atomic wavelength is small compared to the spatial scale of the potential. The phase shift may then be calculated in terms of the action integral along a classical trajectory [17], in the spirit of the WKB approximation or the eikonal approximation in optics. The atomic trajectories, however, are perturbed by the rough potential, which makes an analytical calculation difficult. In the thin phase grating approximation, we assume that the perturbation of the atomic trajectory is small, similar to the Raman-Nath approximation [20,21]. One can then show from the principle of least action that the phase shift is found by integrating the rough potential along the unperturbed trajectories in the flat mirror potential [19]. In the context of atomic scattering at a crystal surface, a similar approach is known as the trajectory approximation [38].

From the phase-shifted wave function (6.1), it is then convenient to calculate the transverse coherence function of the reflected atoms. In the framework of our statistical description of the rough evanescent wave mirror, this function may be introduced in a natural manner [39]

$$\Gamma(\mathbf{R}_1, \mathbf{R}_2) = \langle \psi_r^*(\mathbf{R}_1) \psi_r(\mathbf{R}_2) \rangle, \quad (6.2)$$

where the average $\langle \cdot \rangle$ is taken with respect to the statistical ensemble for the rough surface introduced in Sec. III B. We recall that the coherence function is related to the contrast of the interference pattern one obtains if the mirror is part of an atom interferometer. Also, its Fourier transform with respect to $\mathbf{R}_2 - \mathbf{R}_1$ is equal to the (average) transverse momentum distribution of the reflected atoms.

B. Calculation of the phase shift

In the thin phase grating approximation, the phase shift due to the rough potential $V^{(1)}(\mathbf{r})$ is given by the integral [17,19]

$$\delta\varphi(\mathbf{R}) = -\frac{1}{\hbar} \int dt V^{(1)}[\mathbf{r}^{(0)}(t)], \quad (6.3)$$

where $\mathbf{r}^{(0)}(t)$ is a classical trajectory in the flat potential $V^{(0)}(\mathbf{r})$. This trajectory is uniquely determined by the requirements that it end at the position $(\mathbf{R}, z=h)$ and have the same initial momentum $(\mathbf{P}_i, -p_{zi})$ as the incident atomic plane wave. For the exponential potential of Eq. (2.5), it has the analytical form [30]

$$\mathbf{R}^{(0)}(t) = \mathbf{R}_0 + \mathbf{P}_i t / M, \quad (6.4a)$$

$$z^{(0)}(t) = z_0 + \kappa^{-1} \ln \cosh(t/\tau), \quad (6.4b)$$

where τ is the characteristic time scale of the reflection

$$\tau = \frac{M}{\kappa p_{zi}}. \quad (6.5)$$

The atom reaches the turning point (\mathbf{R}_0, z_0) , with z_0 given by Eq. (2.6), at time $t=0$. As a function of the final position \mathbf{R} , \mathbf{R}_0 is given by

$$\mathbf{R}_0 = \mathbf{R} - \frac{\mathbf{P}_i}{p_{zi}} (h - z_0 + \kappa^{-1} \ln 2), \quad (6.6)$$

where we have used that the final height h is much larger than the decay length $1/\kappa$ of the evanescent wave.

To calculate the phase shift, we insert the Fourier expansion (4.4) of the rough potential $V^{(1)}(\mathbf{r})$ into the integral (6.3). Interchanging the integration order, one may solve the time integral using the variable transformation $t \rightarrow e^{-2t/\tau}$ and the second Euler integral (Eqs. 6.2.1 and 6.2.2 of [34]), with the result

$$\begin{aligned} & \int dt e^{-(\kappa + \kappa') z^{(0)}(t)} e^{i\mathbf{Q} \cdot \mathbf{R}^{(0)}(t)} \\ &= 2\tau e^{-(\kappa + \kappa') z_0} e^{i\mathbf{Q} \cdot \mathbf{R}_0} \beta \left(\frac{\mathbf{Q} \cdot \mathbf{P}_i}{M} \tau, \frac{\kappa'}{\kappa} \right), \end{aligned} \quad (6.7)$$

where the overlap factor β defined in Eq. (5.12) appears again. We now suppose that β in this expression takes the same numerical value as in the matrix element (5.11). This approximation is discussed in more detail in Sec. VI D. It allows us to express the phase shift in terms of the atomic response function $B_{\text{at}}(\mathbf{Q})$ given in Eq. (5.15), with the result

$$\delta\varphi(\mathbf{R}) = - \int \frac{d^2\mathbf{Q}}{(2\pi)^2} S(\mathbf{Q}) B_{\text{at}}(\mathbf{Q}) e^{i\mathbf{Q} \cdot \mathbf{R}_0}. \quad (6.8)$$

The thin phase grating approximation is valid if the rough potential $V^{(1)}(\mathbf{r})$ does not perturb the atomic trajectory very much. For a quantitative estimate, consider an atom in a standing evanescent wave, formed by the interference between the zeroth-order evanescent wave and a scattered light mode. We suppose that this light mode is propagating, in order to find an upper limit for the perturbation of the atomic trajectory. Let $2\pi/Q$ be the period of the standing wave and $\kappa\sigma$ its contrast at the dielectric surface. The optical potential of the standing wave exerts a transverse force on the atom that takes its maximum value at the atomic turning point [cf. Eq. (5.22)]

$$F \lesssim Q \kappa \sigma V_{\text{max}} e^{-\kappa z_0} = Q \kappa \sigma e^{\kappa z_0} \frac{p_{zi}^2}{2M}. \quad (6.9)$$

This force makes the atom move a transverse distance $\sim F \tau^2 / 2M$ during the interaction time τ (6.5). The perturbation of the atomic trajectory is small if this distance is much less than the period of the standing wave. This condition yields the following limit for the rms surface roughness σ :

$$\sigma \ll \frac{8\pi e^{-\kappa z_0} \kappa^2}{\kappa Q^2}. \quad (6.10)$$

For wave vectors Q of the order of a few optical wave vectors, this condition is less restrictive than the limit (5.25) for the validity of the Born approximation. The thin phase grating approximation therefore allows us to go beyond the qua-

specular regime and to cover the experimentally interesting case of a surface roughness larger than the incident atomic wavelength.

C. Calculation of the atomic coherence function

From the result (6.8) for the phase shift, we note that at a given position \mathbf{R} , the phase shift $\delta\varphi(\mathbf{R})$ is a linear combination of surface heights $s(\mathbf{R}')$. It is therefore a Gaussian random process itself [40,41]. This allows us to compute the ensemble average in the coherence function (6.2),

$$\Gamma(\mathbf{R}_1, \mathbf{R}_2) = \langle \psi_r^{(0)*}(\mathbf{R}_1) \psi_r^{(0)}(\mathbf{R}_2) \exp[i\delta\varphi(\mathbf{R}_2) - i\delta\varphi(\mathbf{R}_1)] \rangle, \quad (6.11)$$

with the result

$$\Gamma(\mathbf{R}_1, \mathbf{R}_2) = \Gamma^{(0)}(\mathbf{R}_2 - \mathbf{R}_1) \exp\left[-w + \int d^2\mathbf{Q} \left\langle \frac{dw}{d\mathbf{Q}} \right\rangle \times \exp[i\mathbf{Q} \cdot (\mathbf{R}_2 - \mathbf{R}_1)]\right], \quad (6.12)$$

where $\Gamma^{(0)}(\mathbf{R}_2 - \mathbf{R}_1) \propto \exp[i\mathbf{P}_i \cdot (\mathbf{R}_2 - \mathbf{R}_1)]$ is the coherence function for the flat mirror and $\langle dw/d\mathbf{Q} \rangle$ and w are defined in Eqs. (5.6) and (5.16), respectively. We now discuss the coherence function (6.12) in the quasispecular and diffuse regimes, respectively.

D. Comparison to the Born approximation

In the quasispecular regime where the diffuse reflection probability is small ($w \ll 1$), we may expand the outer exponential in Eq. (6.12), giving a coherence function

$$\Gamma(\mathbf{R}_1, \mathbf{R}_2) = \Gamma^{(0)}(\mathbf{R}_2 - \mathbf{R}_1) \left\{ 1 - w + \int d^2\mathbf{Q} \left\langle \frac{dw}{d\mathbf{Q}} \right\rangle \times \exp[i\mathbf{Q} \cdot (\mathbf{R}_2 - \mathbf{R}_1)] + \dots \right\}. \quad (6.13)$$

Taking the Fourier transform of this result with respect to $\mathbf{R}_2 - \mathbf{R}_1$, we obtain the momentum distribution of the reflected atoms. We observe that this distribution is the sum of a specular peak and a background equal to the differential diffuse reflection probability $\langle dw/d\mathbf{Q} \rangle$ obtained from the Born approximation. An example is shown in Fig. 10(a).

The comparison to the Born approximation allows us to establish a validity condition for the thin phase grating approximation in the quasispecular regime. Recall that we only recover the result of the Born approximation because we have identified the overlap factor β from the phase shift (6.7) with the one appearing in the response function $B_{\text{at}}(\mathbf{Q})$ (5.15). Thus the arguments of β in both cases ($\mathbf{Q} \cdot \mathbf{P}_i \tau/M$ and $\Delta p_z / \hbar \kappa$) must not differ much on the scale of variation of the overlap factor. One can show that their difference arises because the thin phase grating approximation conserves energy only to first order in the in-plane momentum transfer $\hbar \mathbf{Q}$. Expanding the normal momentum change Δp_z to second order in $\hbar \mathbf{Q}$ and comparing the result to $\hbar \kappa$, we find the condition

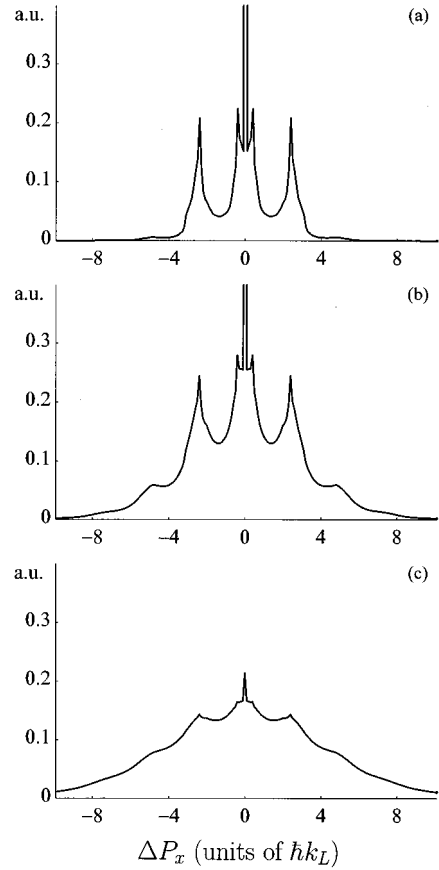


FIG. 10. Transverse atomic momentum distributions for different values of the parameter w . The distributions are one dimensional and calculated in the optical plane of incidence. For a small diffuse reflection probability w , the momentum distribution contains a specular peak superimposed on a diffuse background identical to the inset of Fig. 5. The atomic momentum is given in units of $\hbar k_L$. The incident atoms are plane waves at normal incidence with $p_{zi} = 50\hbar k_L$. (a) $w = 0.5$, (b) $w = 2$, and (c) $w = 5$.

$$\frac{\mathbf{Q}^2}{\kappa^2} \ll 2 \frac{p_{zi}}{\hbar \kappa} \cos^2 \theta_i. \quad (6.14)$$

Since the wave vectors \mathbf{Q} , which are relevant for the diffuse reflection are of the order of a few optical wave vectors (cf. Sec. V C 1), this inequality is satisfied in the semiclassical regime (5.10) and for the typical case that the evanescent wave's decay length is of the order of the reduced optical wavelength. On the other hand, the thin phase grating approximation becomes invalid for a large decay length $1/\kappa$. In this case, the Born approximation may still be used provided, however, that the reflection is quasispecular [cf. Eq. (5.25)].

E. Discussion of the diffuse reflection regime

The diffuse reflection regime corresponds to the limit

$$\langle \delta\varphi(\mathbf{R})^2 \rangle = w \gg 1, \quad (6.15)$$

where the fluctuations of the atomic phase shift are large. We still use the notation w for the integral of the product of the power spectrum and the response function (5.16). In the dif-

fuse regime, however, w no longer appears as a total probability of diffuse reflection, but as a measure of the phase-shift fluctuations.

In the regime (6.15) of large phase fluctuations, we expect the coherence function $\Gamma(\mathbf{R}_1, \mathbf{R}_2)$ to be significantly different from zero only if the positions \mathbf{R}_1 and \mathbf{R}_2 are close. We therefore expand the argument of the exponential in Eq. (6.12) in powers of $\mathbf{Q} \cdot (\mathbf{R}_2 - \mathbf{R}_1)$. The integral over \mathbf{Q} of the first-order term vanishes if we suppose that the differential probability $\langle dw/d\mathbf{Q} \rangle$ is symmetric with respect to the sign of the wave-vector transfer. (Any asymmetry would only lead to a shift of the mean momentum of the reflected atoms, however.) The second-order term of the expansion then yields a coherence function that is Gaussian in $\mathbf{R}_2 - \mathbf{R}_1$:

$$\Gamma(\mathbf{R}_1, \mathbf{R}_2) = \Gamma^{(0)}(\mathbf{R}_2 - \mathbf{R}_1) \exp \left[-\frac{w}{2} \sum_{i,j=x,y} \gamma_{ij} (R_{2i} - R_{1i}) \times (R_{2j} - R_{1j}) \right], \quad (6.16)$$

where the coherence tensor γ_{ij} , with

$$\gamma_{ij} = \frac{1}{w} \int d\mathbf{Q} \left\langle \frac{dw}{d\mathbf{Q}} \right\rangle Q_i Q_j, \quad (6.17)$$

is equal to the average value of the wave-vector transfer components $Q_i Q_j$, weighted by the momentum distribution of the diffusely reflected atoms in the Born approximation. The width δP_{Born} of this distribution has been discussed in Sec. V C 1. The elements of the coherence tensor are therefore of the order of $(\delta P_{\text{Born}}/\hbar)^2$. By Fourier transforming the coherence function (6.16) with respect to $\mathbf{R}_2 - \mathbf{R}_1$, we find that the momentum distribution in the diffuse regime is Gaussian with a width of order

$$\delta P_{\text{diff}} \sim \sqrt{w} \delta P_{\text{Born}}. \quad (6.18)$$

As a consequence of Eq. (6.17), the momentum distribution shows an anisotropy similar to the diffuse reflection probability $\langle dw/d\mathbf{Q} \rangle$.

We note that δP_{diff} given in Eq. (6.18) is the width of an atomic diffraction pattern that would be created by a sinusoidal phase grating with period $2\pi\hbar/\delta P_{\text{Born}}$, if the phase shift of the atomic wave function were modulated with a modulation index \sqrt{w} large compared to unity. This is not surprising because the optical potential above the rough dielectric surface may be understood as an incoherent ensemble of evanescent wave diffraction gratings, each grating corresponding to a given Fourier component of the surface roughness. In this picture, the momentum distribution of the diffusely reflected atoms is obtained by summing the diffraction patterns over the roughness power spectrum. In the quasispecular regime, the diffraction gratings create a small phase modulation of the atomic wave function and only the zeroth and first diffraction orders are populated. The width of the atomic momentum distribution, δP_{Born} , is then given by the range of spatial frequencies that are present in the ensemble of gratings, as discussed in Sec. V C 1. In the diffuse regime, the large phase modulation implies that higher orders are present in the diffraction patterns, up to a maximum dif-

fraction order approximately given by the modulation index. Identifying the modulation index and the rms phase shift fluctuation \sqrt{w} [cf. Eq. (6.15)], we find that the momentum distribution of the diffusely reflected atoms has a width δP_{diff} given by Eq. (6.18).

For an alternative interpretation, consider the angular divergence of the diffusely reflected atomic wave

$$\delta\theta \equiv \frac{\delta P_{\text{diff}}}{P_{zi}}. \quad (6.19)$$

At normal incidence, we may approximate the total diffuse reflection probability w by the result of the corrugated hard wall potential introduced in Sec. V C 2. The estimate (6.18) then yields

$$\delta\theta \sim 2\delta P_{\text{Born}}\sigma_{z_0}/\hbar, \quad (6.20)$$

where σ_{z_0} is the rms roughness of the turning point surface (5.19). Since the correlation length of the turning point surface approximately equals $\hbar/\delta P_{\text{Born}}$ [cf. Eq. (3.11)], its rms slope is of the order of $\delta P_{\text{Born}}\sigma_{z_0}/\hbar$. The angular divergence $\delta\theta$ therefore corresponds to the locally specular reflection from the rough turning point surface.

We give in Fig. 10 a one-dimensional example of the evolution of the atomic momentum distribution as a function of the parameter w . The distributions are calculated by taking the Fourier transform of the coherence function (6.12) with respect to $\mathbf{R}_2 - \mathbf{R}_1$. The surface roughness is assumed to have a constant power spectrum in the wave-vector range $|\mathbf{Q}| \lesssim 5k_L$. Figures 10(a)–10(c) show the broadening of the diffuse part of the momentum distribution for increasing values of w . In the diffuse reflection regime, the distribution is completely dominated by the diffuse part.

VII. LIGHT POLARIZATION AND ATOMIC ZEEMAN SUBLEVELS

So far we have treated the atom as a pure two-level atom with only one lower and one upper state and we have treated the electric field as a scalar field. In this section we outline the modifications of our results when the polarization of the light field and the Zeeman degeneracy of the atomic levels are taken into account. We recall that in the field of laser cooling these ‘‘modifications’’ shifted the main line of interest from Doppler cooling and cooling in intense fields to sub-Doppler cooling with polarization gradients and the still evolving field of subrecoil cooling [42–46]. Polarization gradient cooling mechanisms are not only theoretical suggestions for different and interesting cooling experiments; they are inevitable in situations of laser cooling of real atoms in three dimensions.

The internal sublevel structure of atoms also leads to different and interesting effects in atom optics, by the possibility of tailoring specific potentials for the atomic motion. For example, large-angle diffraction from a triangular potential has been demonstrated by combining a polarization gradient laser field and a magnetic field [47]. Also, atomic interferometry with spatially overlapping trajectories is possible using superpositions of internal states [48]. In closer connection to the present work, the coherent reflection of multilevel

atoms from a light field has recently attracted considerable attention [49–51]. Using numerical integration of the Schrödinger equation, it has recently been shown [52] that incorporation of the multilevel structure leads to larger diffraction probabilities, in agreement with experiments [9,10].

This section of the paper is motivated both by our interest in identifying the different qualitative features emerging when the light polarization and the atomic Zeeman sublevel structure are taken into account and by the obvious need of establishing a connection between our model studied above and the expected outcome of real experiments. We shall stay in the limit of large detuning and low saturation of the atomic transition, and in analogy to Eq. (2.1), the ground-state light shift (2.5) becomes an operator acting only on the ground state

$$\hat{\mathbf{V}} = \frac{d^2}{\hbar\Delta} (\mathbf{d}^- \cdot \mathbf{E}^*) (\mathbf{d}^+ \cdot \mathbf{E}), \quad (7.1)$$

where, in addition to the position dependence, entering through the electric-field vector \mathbf{E} , the light shift is an operator acting on the Zeeman manifold as indicated by the raising and lowering parts of the atomic dipole operator $d\mathbf{d}^\pm$. The matrix elements of the dimensionless operators \mathbf{d}^\pm are given by the Clebsch-Gordan coefficients, and although the excited state is eliminated [Eq. (7.1) couples only the ground states], the potential results from the direct coupling of the ground and excited states by the laser field and the operator depends on the excited-state degeneracy through the values of the Clebsch-Gordan coefficients.

First, we shall consider the reflection of atoms at the light field above a perfectly flat surface. We then take the surface roughness into account, to first order in the scattered light field, and following the approach in Sec. V, the diffuse atomic reflection is calculated in the Born approximation. We refrain from generalizing the thin phase grating approach of Sec. VI to this situation. The problem is similar to the one of semiclassical approaches to sub-Doppler cooling: without surface roughness, different potentials [position-dependent eigenvalues of the light-shift operator (7.1)] are identified, resulting in an ambiguous choice of the classical trajectory and hence a difficulty in consistently accumulating the effect of the potential on the atomic motion; cf. Eq. (6.3).

A. Flat mirror

If we consider a planar dielectric surface and an incident field with the electric-field vector parallel with this surface (TE polarization), we obtain an evanescent wave with its polarization vector pointing along the same direction, e.g., $\mathbf{E}_i = E_0 \mathbf{e}_y$, $\mathbf{K} \parallel \mathbf{e}_x$. It is then convenient to adopt the y direction for the quantization of the internal atomic angular momentum and to introduce the resulting eigenstates $|m\rangle$. Using the Clebsch-Gordan coefficients defined in Fig. 11, we can write out the light-shift potential operator (7.1) in matrix form and, due to our choice of quantization axis, this matrix becomes diagonal with elements

$$\hat{\mathbf{V}}_0(m \rightarrow m) = c_\pi(m)^2 V_{\max} e^{-2\kappa z}, \quad (7.2)$$

where $V_{\max} = d^2 E_0^2 / \hbar \Delta$ is the scalar value of the dipole potential at the surface.

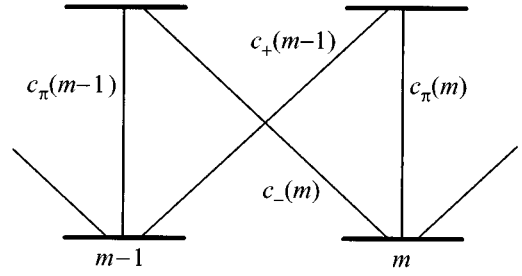


FIG. 11. Transitions among atomic sublevels and our shorthand notation for the Clebsch-Gordan coefficients.

Suppose now that an atom is incident on the evanescent field and that the atom enters in a superposition of the internal eigenstates of $\hat{\mathbf{V}}_0$. The reflection is specular, but the different components acquire different phases and, e.g., an initial state with maximal angular momentum with respect to the z axis, $|m_z = J\rangle$, may be detected in the reflected beam with amplitudes on different m_z states showing interferences as a function of the atomic momentum. The phase shift of the atomic wave for the reflection by any of the potentials (7.2) is known [30], but the only quantities needed for the interference problem are the differences between the phase shifts. Due to the common exponential character of the potentials, their amplitude differences are equivalent to a shift in the location above the dielectric at which they assume identical values. This implies that the wave functions in each potential are also identical up to a shift in the z dependence, which is simply obtained, e.g., from the locations of the different classical turning points (2.6). For different eigenvalues m, m' of the y component of the internal angular momentum, we simply have

$$z_m - z_{m'} = \frac{1}{2\kappa} \ln \left(\frac{c_\pi(m)^2}{c_\pi(m')^2} \right). \quad (7.3)$$

We now match the asymptotic ingoing amplitudes of atoms arriving with the momentum component $-p_z$ along the z axis in an arbitrary internal superposition state

$$|\chi_{\text{in}}\rangle = \sum_m a_m |m\rangle \quad (7.4)$$

and we obtain the internal state of the reflected atoms

$$|\chi_{\text{out}}\rangle = \sum_m a_m \exp[2ip_z(z_{m=0} - z_m)/\hbar] |m\rangle, \quad (7.5)$$

where a common phase factor [the phase shift for reflection at the potential (7.2) with $m=0$] has been omitted.

If the incident atom is in a given internal eigenstate $|m\rangle$, we observe that the reflection is both specular and scalar as in Sec. II. This situation will therefore present the most clear case for studies of the effect of surface roughness on the reflection properties of the mirror.

B. Rough mirror

In the case of the rough mirror, we again focus on the diffusely reflected atomic wave and we note that since the surface roughness implies scattered light with different po-

larization components, the diffuse reflection may be accompanied by changes of the internal state, also in the basis of internal angular momentum with respect to the y axis. We find that the elements of the Raman matrix that generalizes the rough potential $V^{(1)}$ (4.2) are proportional to the scattered field components with the corresponding polarizations. For example, the matrix element proportional to the field component with σ^- polarization for the diffuse reflection from the $|m=J\rangle$ substate into the $|m=J-1\rangle$ substate is given by

$$\langle J-1 | (\mathbf{d}^- \cdot \mathbf{e}_y) (\mathbf{d}^+ \cdot \mathbf{f}) | J \rangle = c_\pi (J-1) c_-(J) (f_z + if_x) / \sqrt{2}. \quad (7.6)$$

We give in Appendix B, Eq. (B2), the polarization vector \mathbf{f} of the scattered light, to first order in the surface roughness. We note from its expression that the light scattered in the optical plane of incidence (the x - z plane) remains polarized parallel to the y direction. Equation (7.6) therefore implies that the atomic reflection is scalar in this plane. However, this property breaks down if we take into account higher-order terms of the surface corrugation in the scattered light field [53].

We generalize the Born approximation applied in Sec. V and we first identify the initial and final states $\psi_{i,f}$ as internal Zeeman substates $|m_{i,f}\rangle$. For convenience we introduce the shorthand notation

$$c_{i,f} = c_\pi (m_{i,f})^2. \quad (7.7)$$

The initial and final states are taken as eigenstates of the zeroth-order potential as discussed above. Transitions among states with different m values are induced by the surface roughness, and to lowest order we note the ‘‘selection rule’’ $\Delta m = 0, \pm 1$.

For the diffuse reflection probability, we need to calculate the matrix element (5.8) between the wave functions $\phi_{p_{z_i,f}}$. The wave functions are known as in the scalar case, and this overlap is again obtained in closed form. In the case of identical light shifts, one recovers the result for the scalar case (5.11), with the turning point z_0 replaced by $z_f = z_i = z_{m_{i,f}}$. This is not surprising since the Clebsch-Gordan coefficients $c_i = c_f$ simply shift the dipole potentials, and hence the wave functions $\phi_{p_{z_i,f}}$ by a common distance for both states.

On the other hand, if the atom is coupled to a state with a different light shift, we find a correction to the matrix element (5.11). Assuming again the semiclassical limit $p_{z_i,f} \gg \hbar \kappa$, it takes the form

$$\begin{aligned} & \langle \phi_{p_{z_f}, m_f} | \exp[-(\kappa + \kappa')z] | \phi_{p_{z_i}, m_i} \rangle \\ &= (2\kappa)^{-1} \exp[-(\kappa + \kappa')z_i] \beta \left(\frac{\Delta p_z}{\hbar \kappa}, \frac{\kappa'}{\kappa} \right) \mathcal{F}(z_f - z_i), \end{aligned} \quad (7.8)$$

where the last factor depends on the distance between the turning points of the initial and final states, the momenta $p_{z_i,f}$, and the decay constant κ' and is given in the Appendix, Eq. (A13). We have the following expression for the matrix element (7.8) in the particular case that the momen-

tum difference vanishes and the decay constants are equal (Eq. 15.3.1 of Ref. [34]), i.e., $\Delta p_z = 0$, $\kappa' = \kappa$:

$$\begin{aligned} & \langle \phi_{p_{z_f}, m_f} | \exp[-(\kappa + \kappa')z] | \phi_{p_{z_i}, m_i} \rangle \\ &= (2\kappa)^{-1} \exp[-\kappa(z_i + z_f)] \frac{\hbar \kappa \sin[p_{z_i}(z_f - z_i)/\hbar]}{p_{z_i} \sinh[\kappa(z_f - z_i)]}. \end{aligned} \quad (7.9)$$

It shows that the overlap integral is maximum if the turning points z_i and z_f coincide. As a function of the difference $z_f - z_i$, it oscillates with a period equal to the incident atomic wavelength $2\pi\hbar/p_{z_i}$. If the turning point z_i becomes separated from z_f by more than the decay length of the potential, the overlap is still oscillating at the same period, but it decreases proportional to $\exp(-\kappa|z_i - z_f|)$. At normal incidence, where the momentum change Δp_z is close to zero, we therefore expect that the atomic scattering into a different sublevel is reduced if the corresponding light shifts differ much.

It is interesting to note that for a fixed distance between the turning points, there are particular values of the incident atomic momentum where the matrix element (7.9) is zero:

$$p_{z_i}^{(l)} = \frac{\pi l \hbar}{|z_f - z_i|}, \quad l = 1, 2, \dots \quad (7.10)$$

In these situations, the diffuse reflection probability into the Zeeman sublevel m_f vanishes because the stationary wave functions $\phi_{p_{z_i,f}}$ in the overlap integral are shifted in such a way that they are approximately in phase quadrature.

More generally, we have found that the overlap (7.8) is peaked if the classical turning points z_i and z_f coincide. This Franck-Condon principle leads to a favored transfer of kinetic energy between the normal and in-plane components equal to the potential-energy difference at the common turning point.

As an example, consider a final state $|p_{z_f}, m_f\rangle$ in a stronger potential than the initial state, $c_f > c_i$. The overlap is then maximum for a final momentum $p_{z_f} \approx (c_f/c_i)^{1/2} p_{z_i}$ larger than p_{z_i} . For atoms incident at an oblique angle, this enhances in-plane momentum transfers $\hbar \mathbf{Q}$ antiparallel to the incident momentum \mathbf{P}_i because they are associated with an increase of p_{z_f} . Momentum transfers parallel to \mathbf{P}_i (in the ‘‘forward’’ direction) are suppressed because they lead to a negative normal momentum transfer $\Delta p_z < 0$. The momentum distribution of the atoms scattered into a different sublevel may therefore differ significantly from the scalar results shown in Figs. 7 and 8.

In summary, we are able to compute, within the Born approximation, the momentum distribution of the diffusely reflected atoms in the different Zeeman sublevels. The internal state transitions are driven by the different polarization components of the optical near-field given by the expression (B2) in Appendix B. We already noted that within the x - z scattering plane the light is polarized along the y axis and an important difference from the scalar case is indeed the correlation between the diffuse reflection in different directions and the change of internal sublevel. A detection of the internal state content of atoms reflected in different directions may hence serve as a probe of the polarization structure of the optical near field. In addition, the atomic scattering behavior

tween different sublevels is accompanied by a conversion between internal and kinetic energy. With respect to the scalar case, this may significantly change the momentum distribution of the atoms that are scattered between different Zeeman substates.

VIII. CONCLUSION

In summary, we have studied the scattering of atoms from the optical potential created by both an evanescent and scattered light field above a rough dielectric surface. The atomic scattering is sensitive to height variations of the dielectric surface at the scale of the incident atomic wavelength λ_{dB} and spatial frequencies of the roughness up to a few optical wave vectors are relevant. The momentum distribution of the scattered atoms, averaged over a large number of samples of the rough surface, gives access to the power spectrum of the surface roughness in this spectral range.

Our results have important experimental ramifications. Consider, for instance, an atom interferometer where the atoms are reflected at an evanescent wave mirror in one arm and interfere with an atomic reference beam. Due to the distortion of the reflected atoms' wave front, the contrast \mathcal{A} of the ensemble-averaged atomic interference pattern is reduced by a Debye-Waller-type factor [54] and equals

$$\mathcal{A} = \langle \exp[i \delta\varphi(\mathbf{R})] \rangle = \exp[-\frac{1}{2} \langle \delta\varphi(\mathbf{R})^2 \rangle] = e^{-w/2}, \quad (8.1)$$

which may be shown using the characteristic function for the surface profile $s(\mathbf{R})$ [41]. In the quasispecular regime, the contrast $\mathcal{A} \approx 1 - w/2$ is equal to the probability amplitude of the specularly reflected atoms. For a larger diffuse reflection probability, the fringe contrast and the specular peak decrease exponentially.

Another important prediction of our theory is that even for an isotropic roughness spectrum, the momentum distribution of the reflected atoms shows a significant asymmetry. At normal incidence, the atoms are predominantly scattered parallel to the propagation direction of the evanescent wave. At a finite angle of incidence, the asymmetry of the momentum distribution depends on the relative orientation of the optical and atomic planes of incidence: the approximate conservation of normal momentum causes the scattering to occur predominantly perpendicular to the atomic plane of incidence. Furthermore, when the light polarization and the atomic Zeeman degeneracy are taken into account, the populations of different internal states become correlated with the scattering directions and the conversion between internal and kinetic energy may lead to a significant increase of the normal momentum transfer.

Our results suggest that the diffuse atomic reflection from the evanescent wave above a corrugated dielectric surface may serve as a probe of the surface quality at the scale of the atomic wavelength. We note that this surface probe is complementary to optical near-field microscopy [35–37]. Indeed, the turning point surface we introduced to interpret the atomic scattering is a particular iso-intensity surface that may be obtained directly by a scanning near-field optical microscope operated in the constant-intensity mode. The atomic scattering presents two advantages because the perturbation

of the optical near field due to the atoms is negligibly small and because the atoms are sensitive in a straightforward way to the light polarization of the near field.

The van der Waals interaction, which has recently been investigated by the reflection of atoms at an evanescent wave mirror [55], introduces an additional rough potential related to the surface roughness. But for typical turning point distances, one may show [56] that it is small compared to the rough optical potential we considered here. In the case of multilevel atoms, there is another consequence of the van der Waals interaction: the phase shifts of specularly reflected Zeeman substates are modified because they probe this interaction at different distances.

Finally, we did not consider the optical potential $V^{(2)}$ associated with the intensity $|E^{(1)}|^2$ of the light scattered into the half space above the dielectric. A model of the interaction between the atom and, e.g., the far-field speckle pattern would be a natural extension of the present work.

ACKNOWLEDGMENTS

We acknowledge valuable discussions with A. Sentenac, R. Carminati, and J.-J. Greffet. K.M. thanks the Université de Paris-Sud (Orsay) for its hospitality and financial support. This work was supported by the Ultimatech program of the Centre National de la Recherche Scientifique (France) and the European Union Human Capital and Mobility program under Grant No. ERB CHRX CT920057.

APPENDIX A: EXACT SOLUTIONS FOR THE EXPONENTIAL POTENTIAL

1. Wave functions

We give here the solution $\phi_{p_{zi}}(z)$ of the one-dimensional stationary Schrödinger equation with an exponential potential

$$-\frac{\hbar^2}{2M} \frac{d^2 \phi_{p_{zi}}}{dz^2} + V_{\text{max}} e^{-2\kappa z} \phi_{p_{zi}}(z) = \frac{p_{zi}^2}{2M} \phi_{p_{zi}}(z). \quad (A1)$$

Assume for simplicity that the exponential potential applies for all values of z , positive and negative. The region of large negative z is classically forbidden since the potential becomes larger than the atomic energy. The solution of Eq. (A1) that vanishes in this region reads [28–30]

$$\phi_{p_{zi}}(z) = \sqrt{\frac{P}{\pi}} \sinh \pi P K_{iP}(P_{\text{max}} e^{-\kappa z}). \quad (A2)$$

The (real) function $K_{iP}(x)$ is a modified Bessel function of the second kind [34]. The wave function (A2) is normalized to a sine wave of unit amplitude in the asymptotic region. The positive numbers P and P_{max} are given by

$$P = \frac{p_{zi}}{\hbar \kappa}, \quad P_{\text{max}} = \sqrt{\frac{2M V_{\text{max}}}{\hbar^2 \kappa^2}}. \quad (A3)$$

2. Differential scattering probability

We first derive the expression (5.4) for the scattering cross section in the first Born approximation. To this effect, we normalize the wave functions (A2) in a large box of length L (in the z direction) and area A (parallel to the average mirror surface). Imposing periodic boundary conditions in the x and y directions and an infinite hard wall at $z=L$, the atomic momenta are quantized with spacings

$$\delta p_{x,y} = \frac{2\pi\hbar}{\sqrt{A}}, \quad \delta p_z = \frac{\pi\hbar}{L} \quad (\text{A4})$$

and the final density of states equals

$$\frac{dn}{dE_f} = M |\mathbf{p}_f| \frac{AL}{4\pi^3\hbar^3} d\Omega_f. \quad (\text{A5})$$

The normalization factor for the wave functions $\psi_{i,f}(\mathbf{r})$ (5.1) then equals $\sqrt{2/AL}$ and the probability current of the incident wave is $j_i = |\mathbf{p}_i|/2MAL$. We now insert these expressions into the usual formula for the differential cross section in the Born approximation

$$\frac{d\Sigma}{d\Omega_f} = \frac{2\pi}{\hbar} \frac{1}{j_i} |\langle \tilde{\psi}_f | V_1(\mathbf{r}) | \tilde{\psi}_i \rangle|^2 \frac{dn}{dE_f d\Omega_f}, \quad (\text{A6})$$

where $\tilde{\psi}_{i,f}$ are normalized wave functions. The dimensions A, L of the box then drop out, as they should, and we find the cross section (5.4).

This scattering cross section has to be normalized because the atom interacts with a potential that extends over an infinite surface, in contrast to the spatially localized potentials of usual scattering theory. A (differential) probability of diffuse reflection $dw/d\Omega_f$ is defined by normalizing the number of scattering events per unit time and unit element of solid angle $dN_{sc}/d\Omega_f dt$ to the number of incident atoms per unit time dN_i/dt . According to the definition of the cross section, we have

$$\frac{dN_{sc}}{d\Omega_f dt} = j_i \frac{d\Sigma}{d\Omega_f}, \quad (\text{A7})$$

where j_i is the incident atomic probability current. The number of incident atoms per unit time is infinite if we consider incident plane waves and a scattering potential that extends over the whole x - y plane. Taking the limit of a large, finite mirror surface with area A , it is given by

$$\frac{dN_i}{dt} = j_i A \cos\theta_i, \quad (\text{A8})$$

where $\cos\theta_i$ is the projection of the surface normal onto the direction of the incident atoms. The differential probability of diffuse reflection is therefore given by

$$\frac{dw}{d\Omega_f} = \frac{1}{A \cos\theta_i} \frac{d\Sigma}{d\Omega_f}. \quad (\text{A9})$$

We shall also express the solid angle element $d\Omega_f$ in terms of the atomic in-plane wave-vector transfer element $d\mathbf{Q}$:

$$d\Omega_f = \frac{\hbar^2 d\mathbf{Q}}{|\mathbf{p}_f|^2 \cos\theta_f}. \quad (\text{A10})$$

Using energy conservation (5.3), one finds expression (5.5).

3. Matrix element

The matrix element (5.8) involves the wave functions $\phi_{p_{z_i,f}}(z)$, which correspond to asymptotic momenta $p_{z_i,f}$ and (for scattering into another Zeeman substate) potential magnitudes $c_{i,f} V_{\max}$. We make the variable transformation

$$z \mapsto u = \sqrt{c_f} P_{\max} e^{-\kappa z}. \quad (\text{A11})$$

The matrix element then leads to an integral of the form

$$\mathcal{I}(P_i, P_f, b, \gamma) = \int_0^\infty du u^{\gamma-1} K_{iP_f}(u) K_{iP_i}(bu), \quad (\text{A12})$$

where $P_{i,f}$ are related to $p_{z_i,f}$ by Eq. (A3). The parameters γ, b are defined as $\gamma = (\kappa + \kappa')/\kappa$ and $b = (c_i/c_f)^{1/2}$. The integral (A12) equals (Eq. 6.576.4 of Ref. [57])

$$\begin{aligned} \mathcal{I}(P_i, P_f, b, \gamma) &= \frac{2^\gamma b^{iP_i}}{8\Gamma(\gamma)} \Gamma\left(\frac{\gamma}{2} + i\frac{P_f - P_i}{2}\right) \Gamma\left(\frac{\gamma}{2} - i\frac{P_f - P_i}{2}\right) \\ &\times \Gamma\left(\frac{\gamma}{2} + i\frac{P_f + P_i}{2}\right) \Gamma\left(\frac{\gamma}{2} - i\frac{P_f + P_i}{2}\right) \\ &\times {}_2F_1\left[\frac{\gamma}{2} - i\frac{P_f - P_i}{2}, \frac{\gamma}{2} + i\frac{P_f + P_i}{2}; \gamma; 1 - b^2\right], \end{aligned} \quad (\text{A13})$$

where ${}_2F_1$ is the hypergeometric function [34]

$$\begin{aligned} {}_2F_1[\alpha_1, \alpha_2; \gamma; x] &= \frac{\Gamma(\gamma)}{\Gamma(\alpha_1)\Gamma(\alpha_2)} \\ &\times \sum_{n=0}^{\infty} \frac{\Gamma(\alpha_1+n)\Gamma(\alpha_2+n)}{\Gamma(\gamma+n)} \frac{x^n}{n!}. \end{aligned} \quad (\text{A14})$$

For $b=1$, the hypergeometric function in Eq. (A13) reduces to unity. We note that in this case, one may easily compute the integral (A12) using an integral representation for the Bessel K function (Eq. 9.6.24 of [34]).

We obtain the result (5.11) by taking the semiclassical limit $P_{i,f} \gg 1$ in Eq. (A13). The calculation is carried out using the asymptotic expansion of the gamma function (Eq. 6.1.41 of [34]) and expanding the normalization factor of the wave functions (A2).

In the case of Zeeman sublevels with different light shifts, the factor $\mathcal{F}(z_f - z_i)$ has the form

$$\begin{aligned} \mathcal{F}(z_f - z_i) &= \left(\frac{p_{z_f}^2}{p_{z_i}^2} e^{2\kappa(z_f - z_i)} \right)^{ip_{z_f}/\hbar\kappa} \\ &\times {}_2F_1\left[\alpha_1, \alpha_2; \frac{\kappa + \kappa'}{\kappa}; 1 - \frac{p_{z_f}^2}{p_{z_i}^2} e^{2\kappa(z_f - z_i)}\right], \end{aligned} \quad (\text{A15})$$

with α_1, α_2 given by

$$\alpha_{1,2} = \frac{\kappa + \kappa'}{2\kappa} - i \frac{P_{zf} \pm P_{zi}}{2\hbar\kappa}. \quad (\text{A16})$$

The factor $\mathcal{F}(z_f - z_i)$ is real for real κ' ; this follows from the property

$${}_2F_1[\alpha_1, \alpha_2; \gamma; x] = (1-x)^{\gamma-\alpha_1-\alpha_2} {}_2F_1[\gamma-\alpha_1, \gamma-\alpha_2; \gamma; x] \quad (\text{A17})$$

of the hypergeometric function (Eq. 15.3.3 of [34]).

APPENDIX B: POLARIZATION OF THE SCATTERED LIGHT

The scattering of polarized light at a rough surface may be calculated by an extension of the Rayleigh approximation of Sec. III [25,53]. The boundary conditions for the electromagnetic field are the continuity of the tangential components of the electric- and magnetic-field vectors across the surface.

For light with arbitrary polarization, the Fourier component $\mathbf{E}^{(1)}(\mathbf{K}')$ of the transmitted field to first order is linearly related to the electric-field vector $E_0 \mathbf{e}_0$ of the zeroth-order evanescent wave, according to [25]

$$\mathbf{E}^{(1)}(\mathbf{K}') = E_0 f(\mathbf{K}') \mathbf{f}(\mathbf{K}') \kappa S(\mathbf{K}' - \mathbf{K}), \quad (\text{B1})$$

which is similar to the scalar result given in Eq. (3.3) and where the (unnormalized) polarization vector $\mathbf{f}(\mathbf{K}')$ equals

$$\mathbf{f}(\mathbf{K}') = \mathbf{e}_0 - \frac{(\mathbf{k}'_1 \cdot \mathbf{e}_0) \mathbf{k}'_n}{(\mathbf{k}'_1 \cdot \mathbf{k}'_n)}. \quad (\text{B2})$$

In this expression, $\mathbf{k}'_1 = (\mathbf{K}', i\kappa')$ is the (three-dimensional) wave vector of the scattered light wave above the plane $z=0$, with κ' defined in Eq. (3.2), and $\mathbf{k}'_n = (\mathbf{K}', k'_n)$ where $-k'_n$ is the normal component of the scattered wave vector below the plane $z=0$:

$$k'_n = + \sqrt{n^2 k_L^2 - |\mathbf{K}'|^2}, \quad (\text{B3})$$

and the imaginary part of the square root is determined by $\text{Im} k'_n > 0$. In the case of a TE-polarized light wave incident in the x - z plane with $\mathbf{K} = K_x \mathbf{e}_x$ and polarization vector $\mathbf{e}_0 = \mathbf{e}_y$, the light scattered in the optical plane of incidence $\mathbf{K}' = K'_x \mathbf{e}_x$ remains TE polarized since the second term in Eq. (B2) vanishes and the polarization vector $\mathbf{f}(\mathbf{K}')$ reduces to \mathbf{e}_0 .

-
- [1] V. I. Balykin, V. S. Letokhov, Y. B. Ovchinnikov, and A. I. Sidorov, *Pis'ma Zh. Éksp. Teor. Fiz.* **45**, 282 (1987) [*JETP Lett.* **45**, 353 (1987)].
- [2] M. A. Kasevich, D. S. Weiss, and S. Chu, *Opt. Lett.* **15**, 607 (1990).
- [3] S. Feron *et al.*, *Opt. Commun.* **102**, 83 (1993).
- [4] T. Esslinger, M. Weidemüller, A. Hemmerich, and T. W. Hänsch, *Opt. Lett.* **18**, 450 (1993).
- [5] W. Seifert, R. Kaiser, A. Aspect, and J. Mlynek, *Opt. Commun.* **111**, 566 (1994).
- [6] A. Aspect, C. Henkel, G. Labeyrie, and A. Landragin, in *Coherent and Collective Interactions of Particles and Radiation Beams*, Proceedings of the International School of Physics "Enrico Fermi," Course CXXXI, Varenna 1995, edited by A. Aspect, W. Barletta, and R. Bonifacio (Società Italiana di Fisica, Rome, 1996).
- [7] C. Adams, M. Siegel, and J. Mlynek, *Phys. Rep.* **240**, 143 (1994).
- [8] C. G. Aminoff, A. M. Steane, P. Bouyer, P. Desbiolles, J. Dalibard, and C. Cohen-Tannoudji, *Phys. Rev. Lett.* **71**, 3083 (1993).
- [9] M. Christ, A. Scholz, M. Schiffer, R. Deutschmann, and W. Ertmer, *Opt. Commun.* **107**, 211 (1994).
- [10] R. Brouri, R. Asimov, M. Gorlicki, S. Feron, J. Reinhardt, V. Lorent, and H. Haberland, *Opt. Commun.* **124**, 448 (1996).
- [11] A. Steane, P. Szriftgiser, P. Desbiolles, and J. Dalibard, *Phys. Rev. Lett.* **74**, 4972 (1995).
- [12] P. Szriftgiser, D. Guéry-Odelin, M. Arndt, and J. Dalibard, *Phys. Rev. Lett.* **77**, 4 (1996).
- [13] A. Landragin, C. Henkel, G. Labeyrie, R. Kaiser, N. Vansteenkiste, C. I. Westbrook, and A. Aspect, *Opt. Lett.* **21**, 1591 (1996).
- [14] U. Garibaldi, A. C. Levi, R. Spadacini, and G. E. Tommei, *Surf. Sci.* **48**, 649 (1975).
- [15] G. Armand and J. R. Manson, *Phys. Rev. B* **18**, 6510 (1978).
- [16] N. Garcia and N. Cabrera, *Phys. Rev. B* **18**, 576 (1978).
- [17] P. Storey and C. Cohen-Tannoudji, *J. Phys. (France) II* **4**, 1999 (1994).
- [18] C. Henkel, A. M. Steane, R. Kaiser, and J. Dalibard, *J. Phys. (France) II* **4**, 1877 (1994).
- [19] C. Henkel, J.-Y. Courtois, and A. Aspect, *J. Phys. (France) II* **4**, 1955 (1994).
- [20] R. J. Cook and A. F. Bernhardt, *Phys. Rev. A* **18**, 2533 (1978).
- [21] P. J. Martin, P. L. Gould, B. G. Oldaker, A. H. Miklich, and D. E. Pritchard, *Phys. Rev. A* **36**, R2495 (1987).
- [22] L. Rayleigh, *Proc. R. Soc. London Ser. A* **79**, 399 (1907).
- [23] A. A. Maradudin and D. L. Mills, *Phys. Rev. B* **11**, 1392 (1975).
- [24] F. Toigo, A. Marvin, V. Celli, and N. R. Hill, *Phys. Rev. B* **15**, 5618 (1977).
- [25] G. S. Agarwal, *Phys. Rev. B* **15**, 2371 (1977).
- [26] J.-J. Greffet, *Phys. Rev. B* **37**, 6436 (1988).
- [27] M. Nieto-Vesperinas, *Scattering and Diffraction in Physical Optics* (Wiley, New York, 1991).
- [28] J. M. Jackson and N. F. Mott, *Proc. R. Soc. London Ser. A* **137**, 703 (1932).
- [29] G. Armand and J. R. Manson, *Phys. Rev. Lett.* **43**, 1839 (1979).
- [30] C. Henkel, J.-Y. Courtois, R. Kaiser, C. I. Westbrook, and A. Aspect, *Laser Phys.* **4**, 1040 (1994).
- [31] J. M. Soto-Crespo, M. Nieto-Vesperinas, and A. T. Friberg, *J. Opt. Soc. Am. A* **7**, 1185 (1990).
- [32] R. Carminati and J.-J. Greffet, *J. Opt. Soc. Am. A* **12**, 2716 (1995).

- [33] J.-J. Greffet and R. Carminati, *Ultramicroscopy* **61**, 43 (1995).
- [34] *Handbook of Mathematical Functions*, 9th ed., edited by M. Abramowitz and I. A. Stegun (Dover, New York, 1972).
- [35] J. Cites, M. F. M. Sanghadasa, C. C. Sung, R. C. Reddick, R. J. Warmack, and T. L. Ferrell, *J. Appl. Phys.* **71**, 7 (1992); D. Courjon, C. Bainier, and F. Baida, *Opt. Commun.* **110**, 7 (1994).
- [36] J.-J. Greffet, A. Sentenac, and R. Carminati, *Opt. Commun.* **116**, 20 (1995).
- [37] F. D. Fornel, P. M. Adam, L. Salomon, J. P. Goudonnet, A. Sentenac, R. Carminati, and J.-J. Greffet, *J. Opt. Soc. Am. A* **13**, 35 (1996).
- [38] D. V. Kulginov and N. V. Blinov, *Surf. Sci.* **313**, 120 (1994).
- [39] M. Born and E. Wolf, *Principles of Optics* (Pergamon, London, 1959).
- [40] L. Mandel and E. Wolf, *Optical Coherence and Quantum Optics* (Cambridge University Press, Cambridge, 1995).
- [41] In a more formal way, the result (6.12) may be derived from the characteristic function for the Gaussian random process $s(\mathbf{R})$,
- $$\left\langle \exp i \int d^2 \mathbf{R}' \xi(\mathbf{R}') s(\mathbf{R}') \right\rangle$$
- $$= \exp \left[-\frac{1}{2} \int d^2 \mathbf{R}' d^2 \mathbf{R}'' \xi(\mathbf{R}') \xi(\mathbf{R}'') \langle s(\mathbf{R}') s(\mathbf{R}'') \rangle \right],$$
- choosing the function $\xi(\mathbf{R}')$ as [using Eq. (6.6)]
- $$\xi(\mathbf{R}') = \int \frac{d^2 \mathbf{Q}}{(2\pi)^2} B_{\text{at}}(\mathbf{Q}) e^{-i\mathbf{Q}\cdot\mathbf{R}'} e^{-i(\mathbf{Q}\cdot\mathbf{P}_i/p_{zi})(h-z_0+\kappa^{-1}\ln 2)}$$
- $$\times (e^{i\mathbf{Q}\cdot\mathbf{R}_1} - e^{i\mathbf{Q}\cdot\mathbf{R}_2}).$$
- [42] P. D. Lett, R. N. Watts, C. I. Westbrook, W. D. Phillips, P. L. Gould, and H. J. Metcalf, *Phys. Rev. Lett.* **61**, 169 (1988).
- [43] J. Dalibard and C. Cohen-Tannoudji, *J. Opt. Soc. Am. B* **6**, 2023 (1989).
- [44] A. Aspect, E. Arimondo, R. Kaiser, N. Vansteenkiste, and C. Cohen-Tannoudji, *J. Opt. Soc. Am. B* **6**, 2112 (1989).
- [45] M. Kasevich and S. Chu, *Phys. Rev. Lett.* **69**, 1741 (1992).
- [46] J. Lawall, F. Bardou, K. Shimizu, M. Leduc, A. Aspect, and C. Cohen-Tannoudji, *Phys. Rev. Lett.* **73**, 1915 (1994).
- [47] C. S. Adams, T. Pfau, C. Kurtsiefer, and J. Mlynek, *Phys. Rev. A* **48**, 2108 (1993).
- [48] C. Miniatura, J. Robert, O. Gorceix, V. Lorent, S. L. Boiteux, J. Reinhardt, and J. Baudon, *Phys. Rev. Lett.* **69**, 261 (1992).
- [49] R. Deutschmann, W. Ertmer, and H. Wallis, *Phys. Rev. A* **48**, 4023 (1993).
- [50] W. Zhang and D. F. Walls, *Phys. Rev. A* **47**, 626 (1993).
- [51] S. M. Tan and D. F. Walls, *Phys. Rev. A* **50**, 1561 (1994).
- [52] D. Gordon and C. M. Savage, *Opt. Commun.* **130**, 34 (1996).
- [53] M. Nieto-Vesperinas, *J. Opt. Soc. Am.* **72**, 539 (1982).
- [54] N. W. Ashcroft and N. D. Mermin, *Solid State Physics* (Saunders, Philadelphia, 1976).
- [55] A. Landragin, J.-Y. Courtois, G. Labeyrie, N. Vansteenkiste, C. I. Westbrook, and A. Aspect, *Phys. Rev. Lett.* **77**, 1464 (1996).
- [56] C. Henkel, Ph.D. thesis, Université de Paris-Sud (Orsay), 1996 (unpublished).
- [57] I. S. Gradshteyn and I. M. Ryzhik, *Table of Integrals, Series and Products*, edited by A. Jeffrey (Academic, San Diego, 1980).